Computational Materials Today 6 (2025) 100032

Contents lists available at ScienceDirect

Computational Materials Today

journal homepage: www.sciencedirect.com/journal/computational-materials-today

The development and applications of semiclassical initial value representation, a promising tool for tackling quantum dynamics

Jia-Xi Zeng [a], Xin-Zheng Li [a,b,c,*]

[a] State Key Laboratory for Artificial Microstructure and Mesoscopic Physics, Frontier Science Center for Nano-optoelectronics and School of Physics, Peking University, Beijing 100871, People's Republic of China
[b] Interdisciplinary Institute of Light-Element Quantum Materials, Research Center for Light-Elemt Advanced Materials, and Collaborative Innovation Center of Quantum Matter, Peking University, Beijing 100871, People's Republic of China
[c] Peking University Yangtze Delta Institute of Optoelectronics, Nantong, Jiangsu 226010, People's Republic of China

ARTICLE INFO

Keywords:
Semiclassical initial value representation
Vibrational spectroscopy
Non-adiabatic dynamics
Chemical reaction rate

ABSTRACT

In this review we present an overview of the semiclassical initial value representation (SC-IVR) method, which is a powerful and promising tool for studying real-time quantum dynamics. We first introduce the origin, history, and basic ideas of it. Then its developments and applications in recent years are listed and discussed in detail, covering a range of fields including vibrational spectroscopy, correlation functions, reaction rate constants and nonadiabatic dynamics. By exploring and analyzing these different aspects of SC-IVR, we hope to provide a comprehensive foundational introduction and technical guidance for interested readers. We also hope that new inspirations and potential integration with other fields can be stimulated to further extend its applicability.

1. Introduction

Condensed matter systems are composed by interacting electrons and nuclei. Thus, accurate theoretical descriptions of condensed matter ultimately reside on accurate simulations of such a many-body system. In practical calculations, the electronic structures are treated in a quantum mechanical manner by default. Concerning the nuclear degrees of freedom (DOFs), it is sometimes safe to treat the nuclei as classical mass points moving on a potential energy surface (PES) and still get good results [1,2]. Along this route, force-field based, machine-learning potential based, and *ab initio* molecular dynamics (MD) provide plentiful information on the statistical and dynamical properties of the nuclei and had become the standard choice in many applications [3–7]. In recent years, however, with the improvements of molecular simulation methods in all aspects, researches related to nuclear quantum effects (NQEs) have attracted more and more attention. The simplest treatment of these NQEs using the harmonic model can include zero-point energies (ZPEs) at the harmonic level. Other effects such as anharmonicity, interference and tunneling, on the other hand, can also come into sight and have been identified by different experiments [8–13]. They make impacts on many properties like the vibrational spectroscopy, chemical reaction rates, and even the strength of hydrogen bonds [14–21]. As such, appropriate descriptions of those effects are also crucial for understanding many molecular and condensed phase systems, especially those containing light elements, and require new recipes that go beyond standard methods like MD.

So far, many methods have been developed to handle the nuclei with quantum treatment. The most straightforward one is called discrete variable representation (DVR), but it becomes totally impractical for larger systems [22–25]. Other advanced methods fall into different categories according to the theoretical framework they rely on. In some of them, the nuclear wave functions are expressed as combinations of the direct products of "single-particle" functions. These methods include multi-configuration time-dependent Hartree (MCTDH) [26–29], vibrational self-consistent field (VSCF) [30–33] and vibrational configuration interaction (VCI) [32,33]. Using such an expression of the nuclear wavefunctions, the Schrödinger equation is solved, which gives the energy levels of the nuclear states and the evolution of the nuclear wave functions. The computational requirement of these methods, however, also grows exponentially with the total DOFs, which posted a strong limit on their application to complex systems [34].

Another category of methods includes those based on imaginary time. The diffusion Monte-Carlo (DMC) method approaches the nuclear wave functions by the spawn and annihilation of diffusing particles [35–37]. The path-integral based methods, e.g. path integral Monte Carlo (PIMC), centroid molecular dynamics (CMD) and ring

* Corresponding author.
E-mail address: xzli@pku.edu.cn (X.-Z. Li).

https://doi.org/10.1016/j.commt.2025.100032
Received 21 January 2025; Received in revised form 6 March 2025; Accepted 12 March 2025
Available online 4 April 2025
2950-4635/© 2025 Published by Elsevier Ltd. This is an open access article under the CC BY license (http://creativecommons.org/licenses/by/4.0/).

polymer molecular dynamics (RPMD), make accurate quantum statistics by inserting harmonically connected beads and record snapshots of the polymer as samples [38–42]. The latter two also gives approximate real-time dynamics with the trajectories generated. The Instanton method describes tunneling effects by analyzing the stationary phase trajectories in imaginary time [43–47]. These methods have their strengths but also limitations. DMC is very accurate about the ground state but encounters difficulties for excited states with nodes. RPMD suffers from spurious resonances from the harmonic chain frequencies, while CMD has its own curvature problem which is originated from the nonphysical centroid position. Their computational cost all grow heavily at low temperatures where a large number of beads are required [41,42]. Instanton works very well in specific situations but the limited consideration of paths also limits the accuracy outside these situations.

Apart from the two categories, there are many other methods such as the quantum transition state theory (QTST) [48], the nuclear-electronic orbital (NEO) methods [49–51], and the stochastic self-consistent harmonic approximation (SSCHA) [52–55]. The NQEs are taken into consideration in different fashions.

Parallel to the aforementioned methods, the semiclassical initial value representation (SC-IVR, or IVR in short) also shows great potential in dealing with real-time dynamics with NQEs accurately addressed [56,57]. The origin of IVR can be traced back to the first half of the last century [58]. With the great progresses achieved in the last few decades, it has become a powerful tool in the study of dynamics of the nuclei [57,59–62]. Starting from the semiclassical approximation to the quantum propagator [58], the evolution of the nuclear wave function can be reformulated in terms of classical trajectories on the same PES. The transformation from the root-searching form to the initial-value representation has finally made the method realistically available for numerical calculations [56,57]. With the additionally kept information of the action and the phase space volumes, it is capable of describing the quantum nature of nuclei and correctly addressing the NQEs including anharmonicity, ZPE, interference and tunneling, thus being a promising tool based on conventional molecular dynamics.

For practical applications, the calculation of vibrational spectra has been a major area of focus. Great success has been achieved with diverse developments proposed in the last few decades which enhance its numerical behavior and extend its usefulness, including the time-averaging filtering [60,63,64], multiple coherent states [65–67], divide-and-conquer technique [61,68,69], adiabatic switching [70,71] and cross-correlation filter diagonalization [62]. Besides spectral calculation, it is also applicable to many other problems involving the quantum propagator, such as the determination of correlation functions and reaction rate constants [72–74]. Using the formally exact expression of rate constant in terms of flux-side correlation function [75], it can be straightforwardly transformed into a double phase space integral and thus fit into the IVR framework. The real-time dynamics is accurately handled and very precise results can be obtained for different scenarios of the reaction barrier with efficient and accurate method for evaluating matrix elements involving the Boltzmann operator [74,76]. There are also many other extensions proposed to address the thermal operators, including the linearized approximation [77], the classical path approximation [73,78] and the forward–backward propagation method [73].

For nonadiabatic potentials, the IVR method may also be applied with proper treatment of the electronic states. One effective method is to bosonize the electron levels and transform them to classical DOFs [79,80]. They are then treated as coupled oscillators with parameters linked to the nuclear coordinates, resulting in additional virtual coordinates and momenta in the system Hamiltonian. This exact mapping process assures correct treatment of the dynamics of the original nonadiabatic system by propagating the new classical one. In this way the IVR method shows great capability on dealing with nonadiabatic systems [76,77,80–83]. The real-time dynamics of the coupled nuclear and electronic DOFs are accurately addressed, just as in the adiabatic case, which is lacking in many other nonadiabatic extension methods that fail to incorporate coherence (such as those based on path integral molecular dynamics). Moreover, the NQEs are still taken good care of by the method while it can only be roughly estimated in other nonadiabatic trajectory-based methods such as surface hopping. This makes the IVR method very promising for combining the quantum nature of the nuclei and the coupling with electronic states on the same footing.

After the peak around the year of 2000, new developments of the method have continued to emerge steadily. However, a comprehensive review of these advancements seems to be lacking, and here we attempt to give an extensive introduction within the authors' range of knowledge. This paper is organized as follows. In Section 2, we introduce the history and basic ideas of the IVR method. In Section 3, we present the various developments made in the past decades. In Section 4, a brief summary and future perspective is given.

2. History and basic ideas

2.1. The semiclassical approximation

We will start from an adiabatic molecular PES in which the potential energy $V(\mathbf{x})$ and atomic force $\mathbf{F}(\mathbf{x})$ are functions of D coordinates and independent of time. The quantum evolution of the system is guided by the Schrödinger equation,

$$i\hbar\frac{\partial\psi(\mathbf{x})}{\partial t}=\left(-\sum_i\frac{\hbar^2\nabla_i^2}{2m_i}+V(\mathbf{x})\right)\psi(\mathbf{x}), \tag{1}$$

where ∇_i and m_i are the partial derivative and atomic mass of the ith DOF. For clarity and convenience, one can make a mass-scaled transformation of the coordinates,

$$x_i\to\frac{x_i}{\sqrt{m_i}},\quad \nabla_i\to\sqrt{m_i}\nabla_i,\quad \psi(\mathbf{x})\to\frac{\psi(x_1/\sqrt{m_1},\ldots)}{\prod_i\sqrt{m_i}}, \tag{2}$$

which eliminates the existence of masses in the equation,

$$i\hbar\frac{\partial\psi(\mathbf{x})}{\partial t}=\left(-\frac{\hbar^2\nabla^2}{2}+V(\mathbf{x})\right)\psi(\mathbf{x}), \tag{3}$$

while the shape of the potential function has also changed accordingly. The mass-scaled equation can be viewed as a uniform one in which the kinetic energy operator is fixed and only the total dimension and the potential function are system dependent. Any systems with the same scaled potential will present exactly the same quantum dynamics.

Now, with the classical definition of the Hamiltonian function $H(\mathbf{p},\mathbf{q})=\mathbf{p}^2/2+V(\mathbf{q})$, the Schrödinger equation can be rewritten as

$$i\hbar\partial_t\psi(\mathbf{q})=H(-i\hbar\nabla,\mathbf{q})\psi(\mathbf{q}). \tag{4}$$

Its form is analogous to the Hamilton–Jacobi equation,

$$-\partial_t S(\mathbf{q},t)=H\left(\partial_{\mathbf{q}}S(\mathbf{q},t),\mathbf{q}\right), \tag{5}$$

which is a formulation of classical mechanics and thus soluble with Newtonian dynamics of trajectories. In order to build a correspondence between the two equations, we write the wave function in terms of its amplitude and phase,

$$\psi(\mathbf{q},t)=A(\mathbf{q},t)\,e^{iS(\mathbf{q},t)/\hbar}. \tag{6}$$

The phase is denoted also as S because with this formulation the real part of $i\hbar\partial_t$ and $-i\hbar\nabla$ are equal to $-\partial_t S$ and $\partial_{\mathbf{q}}S$, therefore one can expect similar behaviors.

Plugging the formulation into Eq. (3) one get the equations of motions of amplitude and phase,

$$\begin{aligned}\partial_t S+H(\nabla S,\mathbf{q})-\frac{\hbar^2}{2}\frac{\nabla^2 A}{A}&=0,\\ \partial_t A+\nabla S\nabla A+\frac{A\nabla^2 S}{2}&=0.\end{aligned} \tag{7}$$

The first equation is almost the same as the Hamilton–Jacobi equation, with an additional term involving the second derivative of the amplitude. If we assume that A varies slowly with respect to $S/\hbar$, which is the same assumption made in the Wentzel–Kramers–Brillouin (WKB) approximation [84,85], we may get rid of the last term and match the first equation exactly with the Hamilton–Jacobi one. The second equation is simpler to analyze by multiplying $2A$,

$$\partial_t \rho + \nabla(\rho \nabla S) = 0, \tag{8}$$

where $\rho = A^2$. It is exactly the equation of continuity in hydrodynamics with $\nabla S = \mathbf{p} = \mathbf{v}$ provided by the classical correspondence. The approximation of discarding the $\hbar^2 \nabla^2 A/2A$ term is usually called semiclassical approximation or the $\hbar \to 0$ approximation. The $\hbar$ here can be interpreted as a scaling factor that measures the oscillation of phase.

The solution of the semiclassically approximated equations is readily available with classical methods. The Hamilton–Jacobi equation just describes the motion of particles under Newtonian force, with initial momenta $\mathbf{p}_0 = \nabla S(\mathbf{q}_0, 0)$. The time-dependent wave function under semiclassical approximation is

$$\psi_{\mathrm{SC}}(\mathbf{q}_t, t) = \left| \frac{\partial \mathbf{q}_t}{\partial \mathbf{q}_0} \right|^{-1/2} e^{iS_t(\mathbf{p}_0, \mathbf{q}_0)/\hbar} \psi(\mathbf{q}_0, 0), \tag{9}$$

where $\mathbf{q}_t$ is the position at time t of the classically evolved trajectory starting from $\mathbf{q}_0, \mathbf{p}_0$, and $\partial \mathbf{q}_t/\partial \mathbf{q}_0$ is the Jacobi matrix of final coordinates with respect to initial ones. S_t is the classical action of the trajectory,

$$S_t(\mathbf{p}_0, \mathbf{q}_0) = \int_0^t \mathbf{p}_{t'} \dot{\mathbf{q}}_{t'} - H(\mathbf{p}_{t'}, \mathbf{q}_{t'})\, dt'. \tag{10}$$

With the semiclassical propagation of wave function at hand, the approximation of the quantum propagator can be derived from a complete basis set and their evolution. Specifically, if one choose the coordinate basis, the short-time propagator is perfectly suitable for the trajectory based formulation [86],

$$\begin{aligned} \left\langle \mathbf{q} \middle| e^{-i\hat{H}t/\hbar} \middle| \mathbf{q}_0 \right\rangle = \left| 2\pi i\hbar \frac{\partial \mathbf{q}}{\partial \mathbf{p}_0} \right|^{-1/2} \exp\left\{ \frac{(\mathbf{q} - \mathbf{q}_0)^2}{2t\hbar} \right. \\ \left. - \frac{t}{\hbar} \int_0^1 V(\lambda \mathbf{q} + (1-\lambda)\mathbf{q}_0)\, d\lambda \right\} + O(t^2). \end{aligned} \tag{11}$$

This, in the first order of t, is what one gets from trajectories starting from $\mathbf{q}_0$ with momentum distribution $\rho(\mathbf{p}_0) = (2\pi\hbar)^{-D}$. By regarding t_1 as zero and t being $t_2 - t_1$, the relation of Eq. (9) holds between the short-time propagators of any two time points $0 < t_1 < t_2$ that are sufficiently small. Thus it is appropriate to use the initial conditions of fixed position and uniformly distributed momenta. The semiclassical propagator is then

$$\left\langle \mathbf{q} \middle| e^{-i\hat{H}t/\hbar} \middle| \mathbf{q}_0 \right\rangle = \left[(2\pi i\hbar)^D \left| \frac{\partial \mathbf{q}}{\partial \mathbf{p}_0} \right| \right]^{-1/2} e^{iS_t(\mathbf{p}_0, \mathbf{q}_0)/\hbar}, \tag{12}$$

where $\mathbf{p}_0$ is the initial momentum of the trajectory connecting $\mathbf{q}_0$ and $\mathbf{q}_t$ while other quantities have same meanings as mentioned before. It is clear from the formula that the coordinate basis matrix element of the propagator under the semiclassical approximation is determined by the classical trajectory connecting them.

Up to now, we have derived the semiclassical propagator under coordinate basis following the idea of van Vleck [58] in 1928, with updated and more rigorous notations. It is commonly called the van Vleck (VV) propagator in literature. Though the ideas are correct and the result is valid at short times, there are details missing from the derivation. Generally there can be more than one trajectories with the same starting and ending positions, which will violate the single-valuedness of the phase. The points at which such situation happens are called *caustics*. The semiclassical wave function diverges at caustics which cuts off the validity of the semiclassical approximation. In fact, by carefully investigating the behavior of the wave function, an additional factor shall be introduced, and different trajectories need to be summed up [87],

$$\left\langle \mathbf{q} \middle| e^{-i\hat{H}t/\hbar} \middle| \mathbf{q}_0 \right\rangle = \sum_j \frac{\left\| \partial \mathbf{q}/\partial \mathbf{p}_{0j} \right\|^{-\frac{1}{2}}}{(2\pi i\hbar)^{D/2}} e^{iS_t(\mathbf{p}_{0j}, \mathbf{q}_0)/\hbar - i\pi m_j/2}. \tag{13}$$

The integer m_j is called the Maslov index which equals the number of caustics this trajectory encounters. Namely, for each sign change of the Jacobi matrix, the square root gains a $\pi/4$ phase and switches branch when the sign changes back again. This correction is first proposed by Gutzwiller [88] in 1967, who started from the path-integral representation of the real-time propagator and applied the stationary phase approximation. With careful mathematics, he arrived at the correct details. Therefore the propagator is sometimes also called the van Vleck - Gutzwiller (vVG) propagator. Under the path-integral perspective, the propagator between two points are determined by the trajectories that are "nearly" classical, and their contributions are grouped with respect to truly classical ones and taken together to form the factor and index in the expression.

Being an approximation, its accuracy and applicability are definitely of high concern. One may prove by direct calculation that Eq. (13) is exact for potentials no more than quadratic including free particles and harmonic oscillator. This can also be justified by checking that the propagator of those potentials all have uniform amplitudes and the discarded term is always zero, or by noticing that the stationary phase approximation assumes a quadratic expansion of the potential at each point on the trajectory. Thus one may expect a good accuracy with potentials that are almost harmonic. Also, at short times the accuracy is guaranteed by Eq. (11). However, at long times and on highly anharmonic potentials, the accuracy is no longer promised. It is known that for deep tunneling the semiclassical propagator gains significant systematic error [89]. For other cases, it generally appears to behave very well.

2.2. Initial value representation

In the previous section we obtained the vVG propagator, which is theoretically well-defined but not calculable in practice. Even with the computational resources today it is still hard to find all the trajectories connecting two specific positions. A critical improvement is made by W. H. Miller and his coworkers to allow realistic applications [56,90–93]. The semiclassical propagator as an operator can be expressed by its matrix elements,

$$\begin{aligned} e^{-i\hat{H}t/\hbar} &= \int d\mathbf{q} \int d\mathbf{q}_0 \, |\mathbf{q}\rangle \langle \mathbf{q}| \, e^{-i\hat{H}t/\hbar} \, |\mathbf{q}_0\rangle \langle \mathbf{q}_0| \\ &= \int d\mathbf{q} \int d\mathbf{q}_0 \, |\mathbf{q}\rangle \sum_j \cdots \langle \mathbf{q}_0|. \end{aligned} \tag{14}$$

The integrals on positions and the summation actually compose an integral on all classical trajectories with time length t, and each trajectory are included exactly once. It is then possible to represent the measure by different parameters, e.g. by initial positions and momenta. It is mathematically very straightforward that the integral can be transformed to

$$\int d\mathbf{q} \int d\mathbf{q}_0 \sum_j = \int d\mathbf{p}_0 \int d\mathbf{q}_0 \left| \frac{\partial \mathbf{q}}{\partial \mathbf{p}_0} \right|. \tag{15}$$

The semiclassical propagator then takes the form of a phase-space integral [59],

$$\begin{aligned} e^{-i\hat{H}t} = \int d\mathbf{q}_0 \int d\mathbf{p}_0 \left[\left| \frac{\partial \mathbf{q}_t}{\partial \mathbf{p}_0} \right| / (2\pi i\hbar)^D \right]^{1/2} \\ \times e^{iS_t(\mathbf{q}_t, \mathbf{q}_0)/\hbar} \, |\mathbf{q}_t\rangle \langle \mathbf{q}_0|, \end{aligned} \tag{16}$$

where only integrals on initial conditions are involved. This formulation is called the initial value representation (IVR) [56] since everything in the integrand is fully determined by the initial conditions. It is

particularly suitable for numerical computations since the integral can be carried out with sampling, classical dynamics and averaging steps, which fits the classic framework of molecular dynamics very well. This is the very basic formulation of the SC-IVR method, besides which there are other different representations based on initial values and classical trajectories. These include the momentum representation, the mixed representations and the coherent state representation [57,94]. They can be derived from similar semiclassical treatments and are all quantum exact for potentials no more than quadratic.

The coherent state representation developed by Herman and Kluk [57] will be of particular concern here and after for its usefulness. The Herman–Kluk (HK) propagator is

$$e^{-i\hat{H}t/\hbar} = \frac{1}{(2\pi\hbar)^D}\int d\mathbf{p}_0 \int d\mathbf{q}_0 C_t\left(\mathbf{p}_0,\mathbf{q}_0\right) \times e^{iS_t(\mathbf{p}_0,\mathbf{q}_0)/\hbar}\left|\mathbf{p}_t,\mathbf{q}_t\right\rangle\left\langle\mathbf{p}_0,\mathbf{q}_0\right|. \tag{17}$$

Here $\mathbf{q}_t, \mathbf{p}_t, S_t$ have the same meanings as stated in the previous section, while C_t is the Herman–Kluk pre-exponential factor

$$C_t\left(\mathbf{p}_0,\mathbf{q}_0\right) = \sqrt{\frac{1}{2^D}\left|\frac{\partial\mathbf{q}_t}{\partial\mathbf{q}_0} + \Gamma^{-1}\frac{\partial\mathbf{p}_t}{\partial\mathbf{p}_0}\Gamma - i\hbar\frac{\partial\mathbf{q}_t}{\partial\mathbf{p}_0}\Gamma + \frac{i}{\hbar}\Gamma^{-1}\frac{\partial\mathbf{p}_t}{\partial\mathbf{q}_0}\right|}, \tag{18}$$

which is related to the Jacobi matrix of phase-space variables (the monodromy matrix). The coherent states are minimum-uncertainty wave packets,

$$\left\langle\mathbf{x}\middle|\mathbf{p},\mathbf{q}\right\rangle = \left(\frac{\det\Gamma}{\pi^D}\right)^{1/4} e^{-\frac{1}{2}(\mathbf{x}-\mathbf{q})^{\mathrm{T}}\Gamma(\mathbf{x}-\mathbf{q})+\frac{i}{\hbar}\mathbf{p}^{\mathrm{T}}(\mathbf{x}-\mathbf{q})}, \tag{19}$$

where Γ is the width matrix of the coherent state, which may have arbitrary value but need to be positive definite. A common and reasonable choice is to make it coincide with the case of quantum harmonic oscillators, with the force constants evaluated at a specific point such as the potential minima. It makes sense as the motion of individual coherent states becomes exact in the corresponding harmonic potential. The coherent states are localized both in coordinate and momentum space, ensuring a bounded sampling range which helps to avoid numerical issues. Despite the additional systematic error induced at short times [95], its good numerical behavior has made it the most widely used representation of the semiclassical propagator. To date, it is still the standard choice for many applications. It has been derived and justified in various different ways [96–100]. The following sections will also be based on the HK propagator.

2.3. Basic aspects of calculations

For now we have discussed the basic theoretical framework of the SC-IVR method. The quantum propagator is approximated with an integral in phase space involving quantities associated with classical trajectories. Using this propagator it is now viable to calculate any physical quantities that can be expressed by the real-time propagator $e^{-i\hat{H}t/\hbar}$.

For example, the energy spectrum of a reference state $|\chi\rangle$ can be obtained from the Fourier transform of its auto-correlation,

$$\begin{aligned} I_\chi(E) &\equiv \left\langle\chi\middle|\delta\left(E-\hat{H}\right)\middle|\chi\right\rangle \\ &= \frac{1}{\pi\hbar}\mathrm{Re}\int_0^\infty dt e^{iEt/\hbar}\left\langle\chi\middle|e^{-i\hat{H}t/\hbar}\middle|\chi\right\rangle \\ &\equiv \frac{1}{\pi\hbar}\mathrm{Re}\int_0^\infty dt e^{iEt/\hbar}A_\chi(t). \end{aligned} \tag{20}$$

By simply replacing the quantum propagator with the approximated one we arrive at the formula for semiclassical energy spectrum,

$$I_\chi(E) = \frac{1}{(2\pi\hbar)^D}\frac{1}{\pi\hbar}\mathrm{Re}\int_0^\infty dt e^{iEt/\hbar}\int d\mathbf{p}_0\int d\mathbf{q}_0 C_t\left(\mathbf{p}_0,\mathbf{q}_0\right) \times e^{iS_t(\mathbf{p}_0,\mathbf{q}_0)/\hbar}\left\langle\chi\middle|\mathbf{p}_t,\mathbf{q}_t\right\rangle\left\langle\mathbf{p}_0,\mathbf{q}_0\middle|\chi\right\rangle. \tag{21}$$

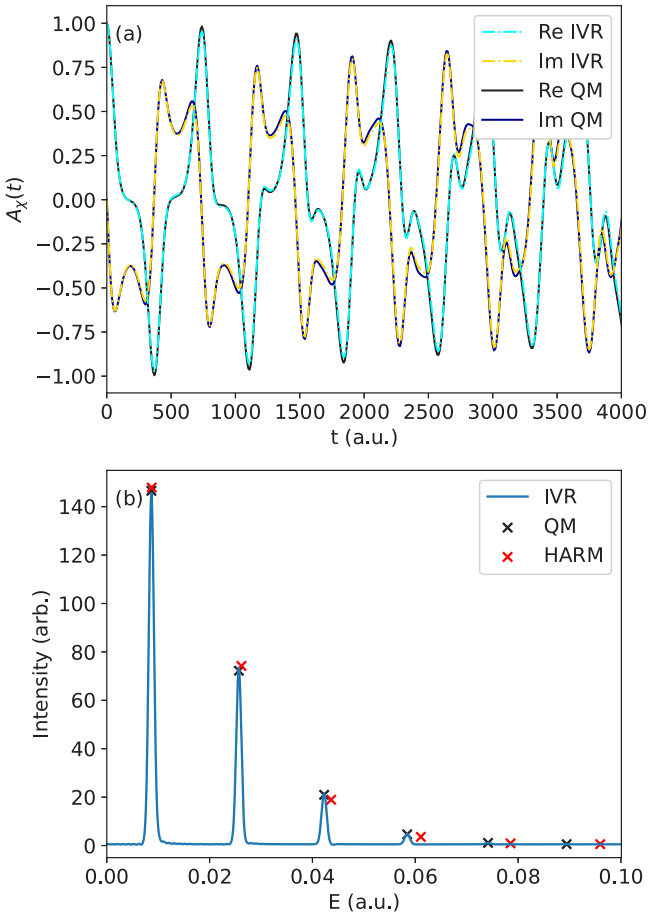

Fig. 1. The auto-correlation function and the energy spectrum of the reference state $|\chi\rangle = \left|p_{\mathrm{eq}},0\right\rangle$ with direct integration of Eq. (21). The upper panel (a) shows the auto-correlation with quantum exact values for comparison. The lower panel (b) shows the energy spectrum with quantum peaks presented as markers, since they have no width at all. Their y coordinates represent the exact intensities $\left|\langle\psi_n\mid\chi\rangle\right|^2$, which are scaled to be comparable with the Gaussian peaks. The results with harmonic approximation (but still quantum) are colored in red for comparison with the exact ones. (For interpretation of the references to color in this figure legend, the reader is referred to the web version of this article.)

The time-domain signal to be transformed is a phase space integral, and the integrand is a function of $\mathbf{p}_0$ and $\mathbf{q}_0$ that can be calculated from classical dynamics.

In principle, one can perform a direct numerical integration to obtain the auto-correlation of the semiclassically propagated reference state, assuming that an infinite supply of computational force is available. This is numerically possible for simple 1-dimensional models such as the Morse oscillator, for which the results are shown in Fig. 1. The potential $V(x) = 0.352\left(1-e^{-0.0208x}\right)^2$ is a good fit of the symmetric stretching mode of the water molecule. The reference momentum is chosen as $p_{\mathrm{eq}} = \sqrt{\omega_0}$, where ω_0 is the harmonic frequency at the minimum. An additional factor $e^{-1.25\times10^{-7}t^2}$ is multiplied in order to avoid oscillatory features around peaks due to the finite propagation time, which will result in a $\Delta E = 5\times10^{-4}$ peak broadening. This example is a pure test of the HK propagator, which yields quantitatively exact results with negligible error. The anharmonicity of the Morse potential is precisely addressed, both in frequency and intensity, as can be seen in Fig. 1(b).

For general multi-dimensional systems, a more practical approach is to utilize the inner product of the initial coherent state with the reference, namely $\left\langle\mathbf{p}_0,\mathbf{q}_0\middle|\chi\right\rangle$ to construct a weight function, and do the numerical integration by Monte Carlo sampling. A common and

convenient approach from earlier times is to define the reference state as a coherent state, since the overlap of coherent states are just Gaussian functions which are easy to compute and sample [63,64].

The same method can be applied to calculate real-time correlation functions,

$$C_{AB}(t) \equiv \mathrm{Tr}\left[\hat{A}e^{i\hat{H}t/\hbar}\hat{B}e^{-i\hat{H}t/\hbar}\right]. \tag{22}$$

By straightforwardly substituting the two propagators the formula for correlation functions under SC-IVR is

$$\begin{aligned} C_{AB}(t) = &\frac{1}{(2\pi\hbar)^{2D}}\int d\mathbf{p}_0\int d\mathbf{q}_0\int d\mathbf{p}_0'\int d\mathbf{q}_0' \\ &\times C_t(\mathbf{p}_0,\mathbf{q}_0)\,C_t'(\mathbf{p}_0',\mathbf{q}_0')\,e^{i\left[S_t(\mathbf{p}_0,\mathbf{q}_0)-S_t'\left(\mathbf{p}_0',\mathbf{q}_0'\right)\right]/\hbar} \\ &\times\left\langle\mathbf{p}_0,\mathbf{q}_0\middle|\hat{A}\middle|\mathbf{p}_0',\mathbf{q}_0'\right\rangle\left\langle\mathbf{p}_t',\mathbf{q}_t'\middle|\hat{B}\middle|\mathbf{p}_t,\mathbf{q}_t\right\rangle. \end{aligned} \tag{23}$$

Due to the two occurrences of the propagator, it is a double integral in phase space and can be evaluated by Monte Carlo sampling of trajectory pairs. For example, by substituting $\hat{A}$ and $\hat{B}$ both with $e^{-\beta\hat{H}/4}\hat{F}e^{-\beta\hat{H}/4}$, one gets a symmetric form for the flux-flux correlation function that exhibits good numerical behavior [74].

While the propagator is based on classically evolved trajectories, there are some extra information that need to be taken care of in addition to standard molecular dynamics. Actions of trajectories are needed for the exponent in Eq. (17), while the pre-exponential factor requires the calculation of the monodromy matrix. The action can be integrated by definition when solving the classical equation of motion, and the monodromy matrix can be solved from the differential equations along the trajectory,

$$\frac{d}{dt}\begin{bmatrix}\frac{\partial\mathbf{q}_t}{\partial\mathbf{q}_0} & \frac{\partial\mathbf{q}_t}{\partial\mathbf{p}_0}\\ \frac{\partial\mathbf{p}_t}{\partial\mathbf{q}_0} & \frac{\partial\mathbf{p}_t}{\partial\mathbf{p}_0}\end{bmatrix} = \begin{bmatrix}0 & \mathbf{I}_D\\ -\left.\frac{\partial^2 V}{\partial\mathbf{q}^2}\right|_{\mathbf{q}_t} & 0\end{bmatrix}\begin{bmatrix}\frac{\partial\mathbf{q}_t}{\partial\mathbf{q}_0} & \frac{\partial\mathbf{q}_t}{\partial\mathbf{p}_0}\\ \frac{\partial\mathbf{p}_t}{\partial\mathbf{q}_0} & \frac{\partial\mathbf{p}_t}{\partial\mathbf{p}_0}\end{bmatrix}. \tag{24}$$

The monodromy matrix and the pre-exponential factor are very important for the HK propagator, and various algorithms are developed to solve it stably [101].

The extra information here gives the IVR propagator true quantum features while it is still based on the same trajectories that may appear in classical molecular dynamics calculations. As presented in Fig. 1(b), the IVR peaks are discrete and sharp. Their widths are very close to the $\Delta E = 5\times10^{-4}$ peak broadening mentioned above, which implies almost perfect delta peaks before broadening. When converted to effective temperature, the average energy of the trajectories can be relatively high, but the phase cancellation keeps the peaks sharp, resulting in an accurate zero-temperature quantum energy spectrum. On the other hand, the peaks from purely classical dynamics will widen at high temperature, and they will fall back to harmonic motions toward 0 K due to the missing ZPE. This makes the IVR spectra fundamentally different from the classical ones, although they both involve classical trajectories and Fourier transforms. This is the reward for the extra computational effort in calculating the additional factors.

When compared to other methods based on classical trajectories such as RPMD and CMD, things become a little bit more complicated. The ring-polymer-based methods give excellent descriptions of quantum statistics, and surpass the IVR framework on problems that depend on only imaginary times. However, when real-time dynamics is involved, they become inaccurate and inefficient, especially at low temperatures. Apart from the problems mentioned in the introduction section, the accuracy of the real-time correlation functions they give is unsatisfactory. In fact, the centroid correlation functions from CMD are just at the level of LSC-IVR [102], a linearized version that has lost many quantum effects when compared to the full IVR approach [103]. Therefore, we note that the most suitable situations for application of the IVR methods are those related with quantum real-time dynamics.

3. Recent developments

In Section 2 we have presented the computational framework of the SC-IVR method, sufficient for its numerical simulations. Such a framework works well on simple systems with a few DOFs, but still lacks practical value at this stage. One serious problem is the computational cost, which grows slower with the number of DOFs than that of the wave function methods, but still in a formidable manner. To extend the applicability of SC-IVR to realistic large systems, many improvements have been developed in the last two decades. Here, we introduce some of them, focussing on their core ideas and the problems they can address.

3.1. Time averaging

The propagation of classical trajectories are very costly for realistic PESs, especially for *ab initio* ones. This is even worse in IVR calculations since as shown in Eq. (24) the Hessian matrix is required for the propagation of the monodromy matrix. To improve the convergence of the numerical integral, the time-averaging (TA) filter is proposed for more efficient utilization of the trajectories and to reduce requirements for samples [60,63,64]. The idea of time-averaging is based on the Liouville's theorem, which asserts that the density in phase space is constant along the classical trajectories of the system. This results in the equivalence of phase space integrals at different times, namely $d\mathbf{p}_0 d\mathbf{q}_0 = d\mathbf{p}_t d\mathbf{q}_t$. As a consequence, any time slice of the evolved trajectories can be regarded as samples with the same weight as evaluated at $t = 0$. Every single trajectory can be considered under this view as a collection of N samples with different lengths, where N is the total steps evolved. By taking all these samples into account, the effective number of trajectories has multiplied by many times without any additional work on propagation.

The expression of energy spectrum using the TA technique is

$$\begin{aligned} I_\chi(E) = &\mathrm{Re}\int d\mathbf{p}_0\int d\mathbf{q}_0\int_0^t dt_1\int_{t_1}^t dt_2 e^{iE(t_2-t_1)} \\ &\times C_{t_2-t_1}\left(\mathbf{p}_{t_1},\mathbf{q}_{t_1}\right)e^{i\left[S_{t_2}(\mathbf{p}_0,\mathbf{q}_0)-S_{t_1}(\mathbf{p}_0,\mathbf{q}_0)\right]/\hbar} \\ &\times\left\langle\chi\middle|\mathbf{p}_{t_2},\mathbf{q}_{t_2}\right\rangle\left\langle\mathbf{p}_{t_1},\mathbf{q}_{t_1}\middle|\chi\right\rangle, \end{aligned} \tag{25}$$

where we have neglected the constant factors and the pre-exponential factor can be obtained using the multiplicity of the monodromy matrix $M(t_2) = M(t_2;t_1)M(t_1)$. In practice it is usually treated with the separable approximation which asserts time separability and unit modulus for the factor [63]. This approximation is seemingly intense as the factor grows rapidly, but it performs very well in practical uses which indicates that the most valuable information are carried by the phase rather than the amplitude. The separable approximation is distinctive for the TA technique because the spectral intensity can be further simplified,

$$\begin{aligned} I_\chi(E) = &\lim_{T\to\infty}\int d\mathbf{p}_0\int d\mathbf{q}_0 \\ &\times\left|\int_0^T dt\left\langle\chi\middle|\mathbf{p}_t,\mathbf{q}_t\right\rangle e^{i\left[Et+S_t(\mathbf{p}_0,\mathbf{q}_0)+\phi_t(\mathbf{p}_0,\mathbf{q}_0)\right]}\right|^2. \end{aligned} \tag{26}$$

It requires only one Fourier transform and is positive definite. This is different from the original formulation which takes average of complex or signed functions. One can clearly see from Fig. 2 that the TA spectrum is well-shaped with a few trajectories while the standard method gives very noisy results. Without the cancellation of different signs, the error must be bounded and the signal-to-noise ratio is guaranteed even with very coarse sampling. This advantage, together with the multiple use of the trajectories, significantly cuts down the number of simulations needed for convergence. The TA technique is also advantageous for its convenience and compatibility with other methods due to the very small cost to modify the calculation process.

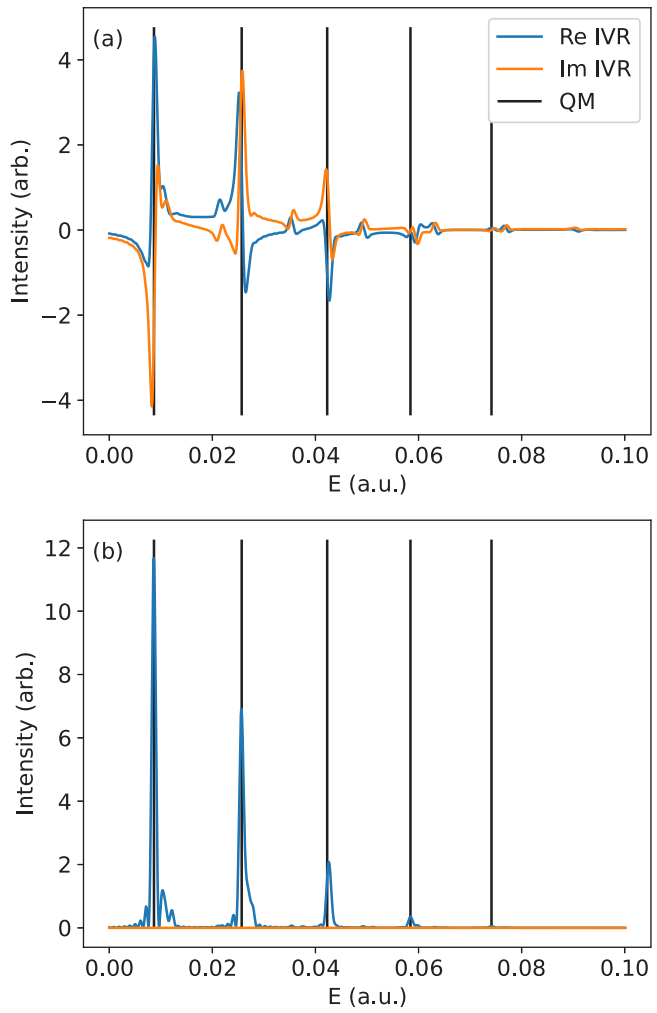

Fig. 2. The energy spectrum of the Morse oscillator with reference state $\left|p_{\mathrm{eq}},0\right\rangle$ and 5 randomly picked trajectories. The results in upper and lower panels belong to standard SC-IVR and TA-SC-IVR, respectively.

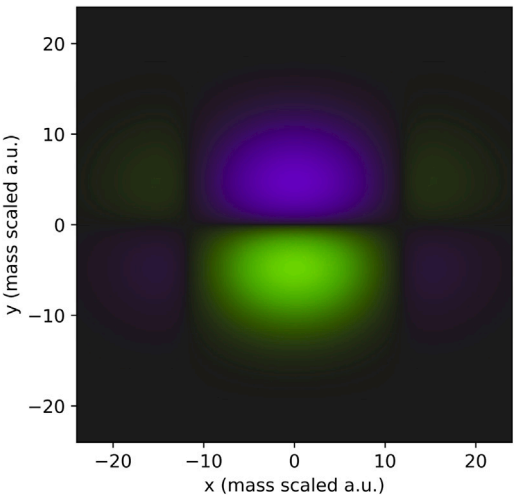

Fig. 3. The wave function plot of the reference state $\left(\left|\mathbf{p}_x,0\right\rangle-\left|-\mathbf{p}_x,0\right\rangle\right)\otimes\left(\left|\mathbf{p}_y,0\right\rangle+\left|-\mathbf{p}_y,0\right\rangle\right)$. The module is represented by brightness while the sign is expressed by color.

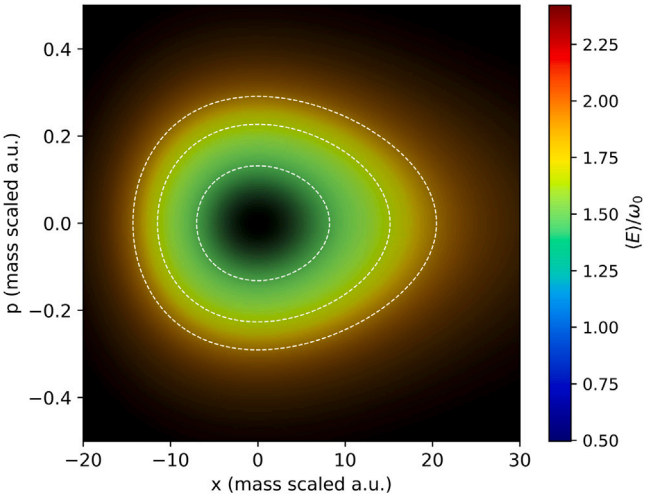

Fig. 4. The contribution of TA spectral intensity from initial conditions in phase space. The brightness is proportional to the total intensity over frequency domain, $P=\int I(\omega)d\omega$, while the color indicates the average energy with respect to harmonic frequency, $\int \omega I(\omega)d\omega/P\omega_0$. The reference state $\left|\sqrt{3\omega_0},0\right\rangle-\left|-\sqrt{3\omega_0},0\right\rangle$ has odd parity, thus the ground state intensity is negligible. Higher even states may have visible contributions due to anharmonicity. The white dashed lines mark the trajectories with classical energy equal to the first 3 eigenvalues, which are approximately $0.497\omega_0$, $1.472\omega_0$, and $2.423\omega_0$.

3.2. Multiple coherent states

In Eq. (21) there are two overlap integrals between coherent states and references. The one based on the initial conditions is bounded by the sampling process if the weight function is chosen properly. The other, however, depends on dynamics and is somewhat unbounded. For the choice of coherent reference states, the overlap is Gaussian distributed in the phase space, with an exponential factor for each DOF. Being distant in any dimension will result in a vanishing value regardless of the others. This makes it exponentially hard for the overlap to keep a finite value with increasing total dimensions. The multiple coherent state (MC) technique, as its name implies, solves the problem by using linear combination of coherent states for Refs. [65,66]. The coherent states are placed near the energy shell in the phase space, maximizing the signals from the trajectories with similar energies. A concise and reasonable choice is to use normal modes and harmonic estimates of energy levels,

$$|\chi\rangle=|\mathbf{p},0\rangle+a\,|0,\mathbf{q}\rangle+b\,|-\mathbf{p},0\rangle+c\,|0,-\mathbf{q}\rangle\,, \tag{27}$$

where $\mathbf{p}^2/2=\hbar\omega\,(n+1/2)=V\,(\mathbf{q})$. The selectivity on different parities can be achieved by appropriate choices of the coefficients [66], as demonstrated by Fig. 3 in which the state has opposite parities along x and y direction. The vibrational peaks from different modes are then distinguishable with such references. By placing more coherent states in the phase space, the time domain signal can be greatly enhanced especially for excited states where the energy shells have larger spans.

The enhanced signal strength and the increased selectivity will significantly reduce the number of trajectories needed for convergence. It becomes more prominent when MC is combined with TA technique. By time-averaging trajectories with desired harmonic energies on each mode, the intensities are enhanced again such that only one trajectory will suffice for spectral analysis [65]. It can be justified from Fig. 4 which clearly demonstrates that the main contributor of intensity are the trajectories near the energy shell. The positivity of the TA spectrum ensures that the peaks are recovered at the right position with those trajectories. This opens up the possibility for semiclassical vibrational spectroscopy of very large molecular systems such as nucleobases [67]. For very expensive potentials such as *ab intio* ones, this is especially useful since the complete phase space integral is prohibited by the cost.

Since the TA and the MC techniques are very easy to implement with negligible computational overhead, the combined TA-MC scheme is very useful in the calculation of vibrational spectra. The change of reference states does not affect the accuracy of the propagator since it is linear. Therefore, the MC technique will not cause any additional error with respect to the original choice of single coherent state. Meanwhile, the TA filtering forces the use of the separable approximation, which might cause unexpected problems. However, up to now no significant issues have been found that strongly break the applicability of this scheme.

3.3. Divide-and-conquer

Most of the difficulties in IVR calculations are caused and intensified by the increase in number of DOFs. The core idea of the divide-and-conquer (DC) technique is to limit the total dimensions under *quantum* consideration, and most of the problems will disappear automatically. This is done by projecting the whole system into lower dimension and write the wave functions and many other expressions in subspace coordinates [61,68,69]. The wave packet is propagated in the subspace which contains the DOFs of interest.

The formula of energy spectrum looks very similar to the standard one,

$$e^{-i\hat{H}t/\hbar} = \frac{1}{(2\pi\hbar)^D}\int d\tilde{\mathbf{p}}_0 \int d\tilde{\mathbf{q}}_0 \tilde{C}_t\left(\tilde{\mathbf{p}}_0,\tilde{\mathbf{q}}_0\right) \times e^{i\tilde{S}_t\left(\tilde{\mathbf{p}}_0,\tilde{\mathbf{q}}_0\right)/\hbar}\left|\tilde{\mathbf{p}}_t,\tilde{\mathbf{q}}_t\right\rangle\left\langle\tilde{\mathbf{p}}_0,\tilde{\mathbf{q}}_0\right|, \tag{28}$$

but with everything under a tilde representing the projection of the corresponding quantities in Eq. (17). It is self-evident how to project a coherent state into lower dimension, and the pre-exponential factor is obtained by projecting the monodromy matrix. The action cannot be directly projected since the potential term in the Hamiltonian is not separable, and special treatment is required.

A common *ad hoc* method is to assume

$$\tilde{V}\left(\tilde{\mathbf{q}}\right) = V\left(\mathbf{q}\right) - V\left(\tilde{\mathbf{q}};\mathbf{q}_{D-\tilde{D}}\right) \tag{29}$$

where $\mathbf{q}_{D-\tilde{D}}$ contains the DOFs outside the subspace. The projected potential in this form is exact for separable cases [61,68]. Strictly speaking, $\tilde{V}$ is not a potential in the subspace because it is not a single-valued function. It accounts for the coupling effects of the classically treated dimensions. Also, the monodromy matrix is not separable and its projection will carry information of those dimensions. In this way the evolution of wave packets is distinguished from quantum dynamics on a PES with reduced dimensions for the additional information inputted. This difference is intrinsic. The quantum vibrational frequencies might be strongly shifted upon dimension reduction due to the neglected coupling between modes, but can be accurately recovered by the DC-SC-IVR with the aid of extra information [68].

For Monte Carlo calculations, the sampling of initial conditions are split into two parts. In the chosen subspace it can still be done with the reference state using standard methods. For other modes, there is no wave function for reference, and a reasonable choice is to assign the corresponding harmonic zero-point motion to each of them, just as in single-trajectory TA-MC calculations. Other intuitive means include a Husimi distribution or harmonic motion with a random initial phase which supply a more extensive exploration of the configuration space. In some cases, part of these DOFs are initially set without kinetic energy so as to avoid noisy spectra [69]. In order to decrease the systematic errors, an appropriate criterion shall be applied to choose the right partition. Some candidate methods utilize the Hessian matrix and the monodromy matrix to judge the extent of coupling [68].

With the number of DOFs under quantum consideration limited to a few, the issues about high-dimensional integration, wave packet overlap and phase oscillation are substantially resolved. The computational cost of each trajectory is nearly the same as standard full-dimensional calculations, but the number of trajectories needed for convergence is lowered to the level of a few DOFs. This greatly suppressed the curse of dimensionality. With other techniques combined like TA and MC, it is possible to handle systems with hundreds of DOFs such as bio-molecules or even larger ones like a solution droplet [67,104]. Is has also been applied to other condensed phase systems such as molecular adsorbates on crystal surfaces, for which it gives good descriptions of the interactions between the adsorbated molecule and the phonons [105].

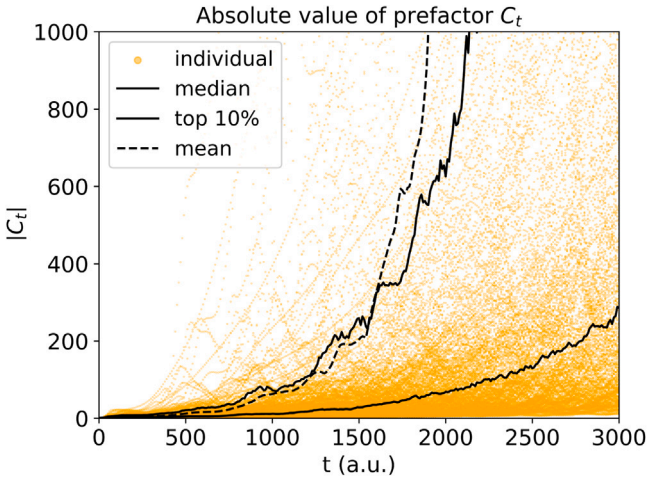

Fig. 5. The distribution of pre-exponential factors of water monomer trajectories with initial conditions drawn from the harmonic Wigner distribution.

The combination of DC and the TA-MC scheme has been applied massively in the calculation of vibrational spectra, especially in the later work of Michele Ceotto and his coworkers, who have become representatives of this branch of IVR method developments. When studying the NQEs in the vibration of large systems, it is the most powerful tool with acceptable accuracy, if not the only one. Yet it will be perfect if the theoretical foundation of the DC technique can be made more solid, reducing its *ad hoc* feature.

3.4. Cross-correlation filter diagonalization

The aforementioned methods have solved most of the problems with their marvelous ideas. However, there are still other difficulties aside from the phase-space integration. The propagation of the classical trajectories and the monodromy matrices have intrinsic hardness owing to the chaotic nature of the dynamics. According to the Liouville's theorem, the phase space volume is conserved during classical evolution. But the shape of the evolved volume unit can be distorted and may cover a very large range. This results in enormous entries of the monodromy matrix, large pre-exponential factors, and bad numerical behavior. In many molecular systems the entries can grow exponentially with time which makes long-time propagation extremely difficult. As can be seen from Fig. 5, the pre-exponential factor grows by almost one order of magnitude between $t = 1000$ and 2000 for a system as simple as a water molecule. These problems are of no significance in conventional molecular dynamics since they do not care about the local densities or the contribution of nearly-classical trajectories, but exert a great influence on SC-IVR calculations. When a trajectory presents such instability, few things can be done apart from direct discard. This not only reduces the sampling efficiency but also raises questions about appropriateness, as part of the phase space is excluded from the integration while no proof of their insignificance is given.

To settle these "classical" difficulties, many techniques are proposed for better numerical stability. The log-derivative method avoids direct calculation of the monodromy matrix, and with further approximations the instability related to chaotic motion can be substantially

removed [101,106]. The adiabatic switching method provides a better sampling of initial conditions with less chaotic behavior [70]. There are also attempts like finite-difference method [107] and practical numerical methods including the Hessian database method which reduces the computational cost of calculating Hessians [108].

Aside from these methods, the cross-correlation filter diagonalization (CCFD) method solves the problems from a different aspect. Most of the instability arise at a typical timescale which depends on the characteristic frequency and the inherent chaos of the system. The chaotic behavior will not become apparent at short times, e.g. within a few periods of vibration. In this case, there will be no extra hardness except for the Hessian calculation with respect to conventional molecular dynamics. By extracting the frequencies from short-time trajectories, one may avoid most of the difficulties without making any approximations and changes in the propagation steps.

With the standard choice of using Fourier transform to obtain the spectrum, the minimal total evolution time is related to the desired resolution as $T \sim 2\pi/\Delta\omega$. A typical total length is $\sim 10^5$ atomic units if one wish to reduce the peak width to a few wavenumbers [60,61,66]. However, with the idea of informatics it is too redundant to propagate for that long. The energy spectrum of a bounded system is discrete, thus the intensity concentrates near the peaks. For a particular reference state, the number of peaks with non-negligible strength is limited to a few, and the spectrum can be characterized by a few numbers such as the peak positions, heights and widths. The information needed to determine this sparse spectrum is much less than that used in Fourier transform [109]. The extra information is not wasted — it confirms the low intensity in irrelevant frequency ranges. But they become unnecessary if we hold the belief that the resulting spectrum only contains sharp and well-shaped peaks. This makes the extraction of accurate frequencies from short trajectories principally feasible. The filter diagonalization method (FDM) is proposed under similar ideas [110] and then further developed for signal processing [111,112].

The CCFD method utilizes an implicit basis composed of propagated reference states which span a Krylov subspace generated by fixed-step propagator $\hat{U} = e^{-i\hat{H}\tau/\hbar}$,

$$\mathcal{K}_N\left(\hat{U}, \{\chi_i\}\right) \equiv \text{span} \bigcup_i \left\{\chi_i, \hat{U}\chi_i, \hat{U}^2\chi_i, \ldots, \hat{U}^{N-1}\chi_i\right\}. \tag{30}$$

The eigenstates can be "almost" found in the subspace,

$$|\psi\rangle \approx \frac{1}{N\left\langle\psi\middle|\chi\right\rangle} \sum_j e^{iE_j\tau/\hbar}\hat{U}^j|\chi\rangle, \tag{31}$$

with much higher precision than mere linear combinations of reference states. The overlap matrix elements of the basis are

$$\begin{aligned} S_{im,jn} &= \left\langle \hat{U}^m\chi_i, \hat{U}^n\chi_j\right\rangle = \left\langle \chi_i\middle|\hat{U}^{n-m}\middle|\chi_j\right\rangle \\ &= \left\langle \chi_i\middle|e^{-i\hat{H}(n-m)\tau/\hbar}\middle|\chi_j\right\rangle \\ &\equiv C_{ij}\left((n-m)\tau\right). \end{aligned} \tag{32}$$

They are just the cross-correlation functions between the reference states, and can be evaluated on the time grid with the SC-IVR method. The cross-correlation function contains oscillating signals from the common eigenstate components of the two reference states,

$$\begin{aligned} C_{ij}(t) &\equiv \left\langle \chi_i\middle|e^{-i\hat{H}t/\hbar}\middle|\chi_j\right\rangle \\ &= \sum_n \left\langle \chi_i\middle|\psi_n\right\rangle e^{-i\omega_n t}\left\langle \psi_n\middle|\chi_j\right\rangle, \end{aligned} \tag{33}$$

and the mission is to recover the parameters from the time-domain signals, especially the frequencies. As implied by the name, it is done with the filter diagonalization method (FDM).

The key idea of FDM is to reuse the cross-correlations with proper structures to make the harmonic inversion numerically stable. Specifically, these functions can also be interpreted as matrix elements of finite-time propagators,

$$U^k_{im,jn} \equiv \left\langle \hat{U}^m\chi_i\middle|\hat{U}^k\middle|\hat{U}^n\chi_j\right\rangle = C_{ij}\left((n+k-m)\tau\right), \tag{34}$$

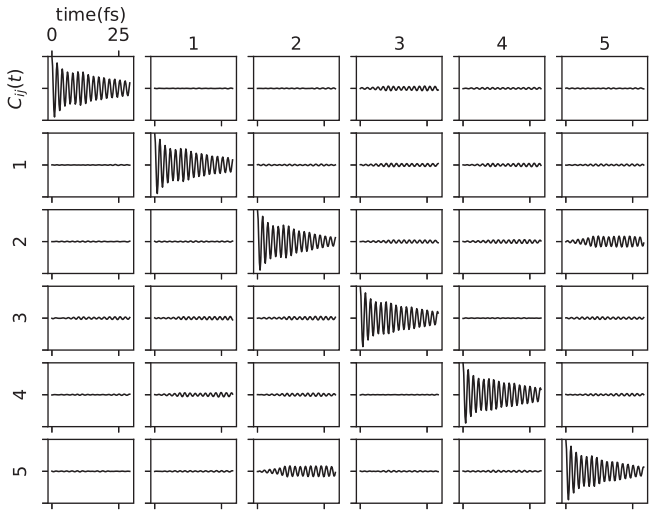

Fig. 6. The real part of cross correlation functions of the 6 reference states related to the 6 OH stretch modes of water trimer, obtained in the calculation of Ref. [62]. The labels on rows and columns denote i, j.

with only a time shift with respect to the overlap matrix. Thus by evaluating the cross-correlation functions one readily obtains the elements of the overlap matrix S and the propagator matrix U^k under the specified basis. Then the eigenvalues of $\hat{U}^k$ can be solved from the generalized eigenvalue problem

$$U^k B = \lambda S B. \tag{35}$$

The frequencies are extracted as $\omega = (i\hbar/k\tau)\ln\lambda$ and the corresponding eigenstates can be expanded with coefficients from B,

$$|\Psi\rangle = \sum_{i,m} B_{im}\hat{U}^m|\chi_i\rangle. \tag{36}$$

In the possible presence of spurious eigenvalues, one may choose multiple values of k to cross check. The matrix elements can all be constructed from the same cross-correlation functions.

The implicit basis becomes overcomplete and linear dependent when N exceeds the number of eigenstate components per reference state. In order to solve the generalized eigenvalue problem in Eq. (35) with good numerical stability, the linear dependency needs to be taken care of. One suitable method is to diagonalize the overlap matrix and filter eigenvectors by eigenvalues. A cutoff threshold is established and the eigenvalues below it are discarded. The problem is then solved in the contracted subspace, with a smaller but linear independent basis.

In order to retain good resolution after the contraction, some modifications to the basis need to be carried out to include the eigenstates in the Krylov subspace. One may choose the Fourier transformed basis [112]

$$\left|\Psi_i\left(\phi_v\right)\right\rangle \equiv \sum_{m=0}^{N-1} e^{im\tau\phi_v}\hat{U}^m|\chi_i\rangle, \tag{37}$$

with ϕ_v lying in a narrow band around the frequency of interest. This will significantly enhance the ratio of the eigenstates with energy in that range and is especially useful when the number of energy levels exceeds that of reference states. One may also use an orthonormal basis which is computed by diagonalizing the Hamiltonian estimated from a coarse Quantum Monte Carlo (QMC) sampling of the potential. This results in good approximations of the eigenstates with which all associated frequencies can be extracted at once [62]. Following the correlation functions in Fig. 6 one can see the imperfection of the references from the leaking of surviving probability as well as their goodness as approximations from the small off-diagonal terms. Any

Table 1
Methane molecule vibrational spectrum calculated with different methods, with the energies presented in wave numbers (cm^{-1}).

Mode	MM[a]	Harm.	TA-SCIVR[b]	DC-SCIVR[b]	AS-SCIVR[c]	CCFD
4_1	3053	3165	3048	3044	3058	3058
2_2	3067	3148	3048	3050		3073
3_1	2949	3043	2948	2964	2950	2948
$1_1 2_1$	2836	2923	2825	2834	2839	2843
1_2	2624	2690	2594	2606	2614	2619
2_1	1535	1574	1529	1532	1530	1537
1_1	1313	1349	1300	1300	1307	1315
MAE		74	12	11	5	4

[a] MULTIMODE result [113].

[b] Previous result by Liberto et al. [68] from the same force field and with Divide-and-Conquer technique, which has the best MAE among listed methods there.

[c] Previous result by Riccardo et al. [70] from the same force field and with Adiabatic Switching technique.

other means will also be useful as long as the coefficients of the eigenstates of interest is not too small in the references.

The CCFD method has a similar core with the TA filtering. In TA each trajectory is treated as $\sim N$ samples, while in CCFD each cross-correlation function supplies $\sim N$ data points which fill in $\sim N^2$ matrix elements. The multiple use of the data increases efficiency. The additional matrix structure makes it feasible to solve directly for the eigenvalues. With proper setup for initial sampling, one trajectory set will suffice for the calculation of all the cross-correlations [62]. With the significantly reduced trajectory length, the overall computational cost of CCFD can be orders of magnitude lower than other SC-IVR-based methods, while no accuracy is lost.

The method has been originally tested on very simple model potentials [114–116], and has recently been successfully applied to realistic molecular PESs with satisfactory outcomes, including the water trimer which is very tricky for both wave function and semiclassical treatments [62]. In Table 1 results using the same methane potential [117] and different methods that belong to the SC-IVR category are listed. The prefixes TA, DC and AS refers to time averaging, divide-and-conquer and adiabatic switching. While the system is pretty chaotic, the short propagation time in CCFD leads to smooth numerical behavior while for long time methods most of the trajectories have to be discarded [68]. The adiabatic switching method solves the chaoticity from a different aspect, for which interested readers are referred to Ref. [70]. The CCFD method also has the power to distinguish symmetry-induced splittings in overtones with correct degeneracy. More details can be found in Ref. [62].

One thing worth notice here is that we assumed an Hermitian Hamiltonian and unitary propagators in our derivations, while old literature often introduce FDM with complex symmetric cases [112]. The derivations are similar except for some minor changes. The Hermitian version works for simple cases where the system will be adequately non-dissipative, while the other must be applied when large damping factors are present. In practice, it is acceptable to assume Hermiticity in most cases even with other tactics applied like the DC technique [62].

3.5. Correction operator

No matter how much numerical efficiency has increased, one problem still exists that the semiclassical propagator is not exact. The quantum propagator obeys the differential equation

$$i\hbar\frac{\partial}{\partial t}\hat{U}(t) = \hat{H}\hat{U}(t). \tag{38}$$

The semiclassical propagator, however, does not satisfy this exactly, and one may define the correction operator as the difference between the two sides [95,118,119].

$$\hat{C}(t) \equiv \left(i\hbar\frac{\partial}{\partial t} - \hat{H}\right)\hat{K}(t), \tag{39}$$

where $\hat{K}(t)$ denotes the propagator in Eq. (17). It can be directly calculated as

$$\begin{aligned}\hat{C}(t) = &\frac{1}{(2\pi\hbar)^D}\int d\mathbf{p}_0\int d\mathbf{q}_0 C_t\left(\mathbf{p}_0,\mathbf{q}_0\right)e^{iS_t(\mathbf{p}_0,\mathbf{q}_0)/\hbar}\\ &\times\Delta\hat{V}\left(\mathbf{p}_t,\mathbf{q}_t\right)\left|\mathbf{p}_t,\mathbf{q}_t\right\rangle\left\langle\mathbf{p}_0,\mathbf{q}_0\right|.\end{aligned} \tag{40}$$

where $\Delta\hat{V}$ is the potential difference operator,

$$\begin{aligned}\Delta\hat{V}\left(\mathbf{p}_t,\mathbf{q}_t\right) = &V\left(\mathbf{q}_t\right) + \nabla V\left(\mathbf{q}_t\right)\cdot\left(\hat{\mathbf{q}}-\mathbf{q}_t\right)\\ &+\left(\hat{\mathbf{q}}-\mathbf{q}_t\right)\cdot\frac{\Gamma^2}{2}\cdot\left(\hat{\mathbf{q}}-\mathbf{q}_t\right)\\ &-\hat{V} - \frac{\mathrm{tr}\Gamma}{2} + i\hbar\frac{\partial_t C_t\left(\mathbf{p}_0,\mathbf{q}_0\right)}{C_t\left(\mathbf{p}_0,\mathbf{q}_0\right)}.\end{aligned} \tag{41}$$

With the correction operator, the exact propagator can be expressed as a Dyson series,

$$\hat{U}(t) = \hat{K}(t) + \frac{i}{\hbar}\int_0^t \hat{U}(t-t')\hat{C}(t'), \tag{42}$$

and the first order correction to the semiclassical propagator is

$$\hat{K}_1(t) = \frac{i}{\hbar}\int_0^t \hat{K}(t-t')\hat{C}(t'). \tag{43}$$

Similar to the original IVR propagator, the corrected one can also be carried out by Monte Carlo sampling [119]. We note that this correction operator has a similar shape with the semiclassical propagator, except that it stops in the middle with an additional potential difference operator. This can be simulated by a hop at time t' with the new position and momentum sampled according to $\left\langle\mathbf{p}',\mathbf{q}'\middle|\Delta\hat{V}\middle|\mathbf{p}_t,\mathbf{q}_t\right\rangle$.

The correction operator provides major accuracy improvements in some cases. However, the large computational cost and complexity renders it not practically useful [119]. A possible compromise is to use the operator as an indicator of the systematic error induced by semiclassical approximation which helps to determine the reliability of the method and the best value of width parameters [120]. In this case it can be calculated together with the semiclassical propagator and only the matrix elements of the potential difference operator requires extra computation.

In addition to the correction operator, there are other methods to correct the systematic error of this semiclassical approach such as higher order correction of the pre-exponential factor or prefactor-free series expansion [100,121]. They also have their problems such as not preserving unitarity. This branch can be partly represented by the work of Eli Pollak, who has explored many systematic modifications of the semiclassical propagator. There are many interesting works but they seem to lack followers, so their potential may not have been fully explored. We will not go deeper here and will focus on the HK propagator in this review. Also as a note, we point out that by adding back the neglected term in Eq. (7) and including the induced non-local potential and force, one arrives at the Bohmian mechanics which is an equivalent representation of quantum mechanics [122–124]. The so called quantum potential vanishes and Bohmian and semiclassical dynamics coincide when particle density keeps uniform in space, which is just the case of constant, linear or quadratic potentials.

3.6. Nonadiabatic systems

The electronic degrees of freedom is very different from the nuclear ones. Electrons are way too quantum to be treated with semiclassical dynamics and we have to turn to external methods which gives potentials for atoms. Under the Born–Oppenheimer approximation, the two kinds of DOFs can be totally separated. But when the approximation breaks down, they need to be considered together. The nonadiabatic potential involves discrete DOFs which come from the electronic states of interest. They do not fit into the framework of SC-IVR as introduced above which deals with continuous ones. A feasible

solution is to convert them with the Meyer–Miller–Stock–Thoss (MMST) mapping [79,80].

Considering the simplest case of two diabatic electronic basis, the Hamiltonian of an electronically nonadiabatic system is of the form

$$H = \frac{\mathbf{P}^2}{2m} + \begin{bmatrix} H_{11}(\mathbf{X}) & H_{12}(\mathbf{X}) \\ H_{21}(\mathbf{X}) & H_{22}(\mathbf{X}) \end{bmatrix}, \tag{44}$$

and it is easy to extend the formalism to general cases. The electronic states can be mapped to excitations of different bosonic modes, which makes a linear transformation from the electronic Hilbert space to the Fock space,

$$|0\rangle_{elec} \to |1_0 0_1\rangle, |1\rangle_{elec} \to |0_1 1_0\rangle. \tag{45}$$

The Hamiltonian can be rewritten as

$$\hat{H} = \sum_{i,j\in\{0,1\}} \hat{a}_i^\dagger H_{ij}(\mathbf{X}) \hat{a}_j, \tag{46}$$

and the state space of the original system is mapped into the subspace with particle number $n_0 + n_1 = 1$. Interpreting the bosonic operators as that of harmonic oscillators, one can transform them to coordinate and momentum operators,

$$\hat{x} = \frac{1}{\sqrt{2}}\left(\hat{a}^\dagger + \hat{a}\right), \hat{p} = \frac{i}{\sqrt{2}}\left(\hat{a}^\dagger - \hat{a}\right). \tag{47}$$

Finally the Hamiltonian can be expressed in terms of classical positions and momenta,

$$\begin{aligned} H =& \frac{\mathbf{P}^2}{2m} + \sum_{i=0}^{1} \frac{H_{ii}(\mathbf{X})}{2}\left(x_i^2 + p_i^2 - 1\right) \\ &+ \frac{H_{12}(\mathbf{X}) + H_{21}(\mathbf{X})}{2}\left(x_1 x_2 + p_1 p_2\right), \end{aligned} \tag{48}$$

where we have used upper-case for nuclear variables and lower-case for electronic ones. Note the -1 in the diagonal terms which makes it different from Ehrenfest mean-field dynamics.

Although initially derived with action–angle variables in a rather heuristic way, the mapping is exact without any approximation introduced. The evolution of the system is perfectly mapped to the dynamics within the single-excitation subspace, with the projection operator

$$\hat{P} \equiv \int d\mathbf{X} |\mathbf{X}, 0\rangle \langle \mathbf{X}, 0| + |\mathbf{X}, 1\rangle \langle \mathbf{X}, 1|. \tag{49}$$

Thus by solving the quantum dynamics of the mapped Hamiltonian one solves the evolution of the original system.

Now the SC-IVR framework can be applied to the Hamiltonian in Eq. (48) which defines classical dynamics. The phase space is composed of the original atomic and mapped electronic dimensions, and the semiclassical propagator is essentially the same as (17),

$$\begin{aligned} e^{-i\hat{H}t/\hbar} =& \int d\mathbf{P}_0 \int d\mathbf{X}_0 d\mathbf{p}_0 d\mathbf{x}_0 C_t e^{iS_t/\hbar} \\ &\times |\mathbf{P}_t\mathbf{p}_t, \mathbf{X}_t\mathbf{x}_t\rangle \langle \mathbf{P}_0\mathbf{p}_0, \mathbf{X}_0\mathbf{x}_0|, \end{aligned} \tag{50}$$

where C_t shall be calculated with the monodromy matrix including both kinds of DOFs. Due to the variable mass terms of the electronic DOFs, it no longer follows Eq. (24) and requires special treatment [125]. The electronic DOFs will not be mass scaled since the corresponding harmonic ground state always have unit width, which leads to the apparent choice of $\Gamma = 1$. The coherent states are superpositions of harmonic eigenstates and are not inside the single-excitation subspace. But their collective motion yields the correct dynamics which keeps the excitation number, assuming the accuracy of the semiclassical propagator. For the calculation of correlation functions, the operators are not directly mapped to x and p but with projection,

$$\hat{O} = \hat{P}\left(\sum_{ij\in\{0,1\}^2} \hat{a}_i^\dagger O_{ij}(\mathbf{X}) \hat{a}_j\right)\hat{P}, \tag{51}$$

in order to avoid furious contributions from other excitation numbers.

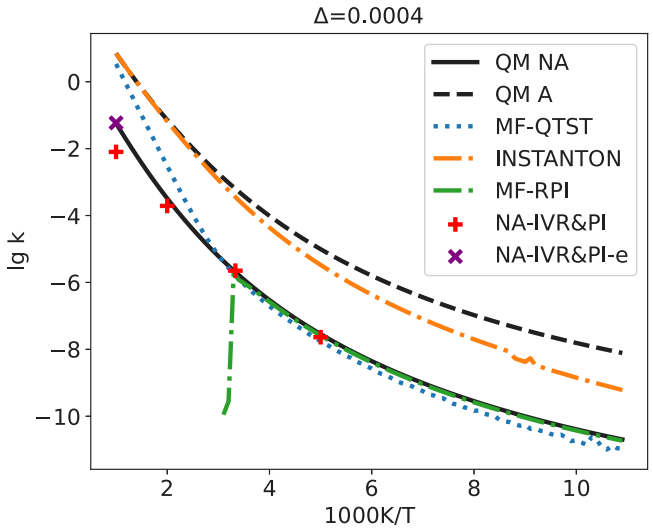

Fig. 7. Arrhenius plot of the avoided crossing model studied in Ref. [76]. The MF- prefix refers to mean-field methods. The sharp turns on Instanton results indicate the break-down point (the crossover temperature). The two NA-IVR & PI methods are based on the same real-time propagator, but with different perspectives of the dividing surface. The large error of NA-IVR & PI in the golden rule limit is caused by the recrossing behavior which magnifies numerical errors.

With the mapping Hamiltonian SC-IVR approach, the quantum dynamics of electronic states coupled with nuclear DOFs can be treated on the same footing. The nonadiabatic effects and the nuclear quantum effects are naturally integrated. The method can be utilized for nonadiabatic wave packet propagation and reaction rate calculation [77,81–83]. For example, recently it has been applied to nonadiabatic reaction models together with path-integral sampling techniques (NA-IVR & PI), which resulted in accurate correlation functions and rate constants for different parameter ranges [76]. Part of the results are shown in Fig. 7. In fact, for the avoided crossing model studied there, the real-time dynamics is always accurate except for very low energy and deep tunneling, no matter if the system is in the golden rule limit or not.

We also note that the mapping Hamiltonian is not the only way to include nonadiabatic effects in the SC-IVR framework. There are other approaches such as Herman–Kluk surface hopping which uses hopping trajectories but keeps the flavor of semiclassical dynamics [126–128]. The optimal method for achieving this remains to be identified.

3.7. Forward-backward propagation

The correlation function of two operators can be calculated by Eq. (23) using trajectory pairs. Though straightforward, it involves a double phase space integral which is more complicated than the single integral in spectral calculations. One way to solve this is to make the linearized approximation which only considers infinitesimally close trajectory pairs whose phases cancel with each other [59,77,129]. This results in the classical Wigner method which only considers individual trajectories in the phase space. However, it is too classical to describe many quantum effects such as interference which involves two separated trajectories [103].

A smart approach to resolve the dilemma is to treat the operators that interrupt propagation as propagators themselves. Here we take the example of flux-side correlation,

$$C_{\mathrm{fs}}(t) = \mathrm{Tr}\left[e^{-\beta\hat{H}}\hat{F}e^{i\hat{H}t/\hbar}\hat{h}e^{-i\hat{H}t/\hbar}\right], \tag{52}$$

which is of fundamental importance in reaction rate theory [75]. The side operator is defined on the reaction coordinate,

$$\hat{h} = \Theta(\xi(\hat{\mathbf{q}})). \tag{53}$$

It can be expressed as a Fourier transform,

$$\hat{h} = \int dp' \frac{e^{ip'\xi(\hat{\mathbf{q}})/\hbar}}{2\pi i\,(p' - i\eta)}, \tag{54}$$

where the numerator can be interpreted as the propagator with time p' and Hamiltonian $-\xi(\hat{\mathbf{q}})$. The classical dynamics is super simple in this case,

$$\dot{\mathbf{q}} = 0, \quad \dot{\mathbf{p}} = \nabla\xi(\mathbf{q}). \tag{55}$$

Thus the effect of this pseudo-propagator is a momentum jump $\mathbf{p} \to \mathbf{p} + p'\nabla\xi(\mathbf{q})$.

Once the side operator is transformed to a propagator, it can be merged with the two propagators beside it to make a single propagation. It comprises three distinct processes: first, forward in time; second, a momentum jump; and finally, backward in time. This can be described by forward–backward trajectories with a momentum change in the middle. Therefore the number of propagators is reduced to one, and only single phase space integration is required,

$$\begin{aligned} C_{\mathrm{fs}}(t) = &\frac{1}{(2\pi\hbar)^D} \int \frac{dp'}{2\pi i\,(p' - i\eta)} \int d\mathbf{p}_0 \int d\mathbf{q}_0 C_{0'}\left(\mathbf{p}_0, \mathbf{q}_0\right) \\ &\times e^{iS_{0'}(\mathbf{p}_0,\mathbf{q}_0)/\hbar} \left\langle \mathbf{p}_0, \mathbf{q}_0 \middle| e^{-\beta\hat{H}} \hat{F} \middle| \mathbf{p}_{0'}, \mathbf{q}_{0'} \right\rangle. \end{aligned} \tag{56}$$

Here we used the time label $0'$ since the forward and backward propagation nominally returns to time zero. This method is referred to as forward–backward IVR (FB-IVR) due to this feature [59,130–135]. The Hamiltonian dynamics of the three processes are all well-defined as well as the action and monodromy matrix.

In the backward propagation, the system evolves as if time is reversed. The classical dynamics is symmetric under time reversal and only the initial momentum and the action shall be negated. For those modes irrelevant to the reaction, the action of forward and backward motion cancels with each other, which reduces the oscillatory character of the integrand. This makes FB very useful for calculating time correlations. The method has been utilized to study correlation functions and chemical reactions including the nonadiabatic ones [82,136–139]. It still holds considerable potential and can provide significant improvements in efficiency. For more details on this branch, we recommend the works of Nancy Makri, Jiushu Shao, and Jian Liu to interested readers [131,132,135–137,140–144]. The research in this field is more divergent and the focus seems to have moved to various different methods that have their own features in the last decade. The more IVR-related part has since become less active.

3.8. Integration of machine learning

The integration of machine learning (ML) into computational physics has been widely explored in recent years. Its strong power in fitting and prediction opens up many new possibilities and brings about new improvements to existing methods. Such changes also take place in the field of IVR calculations.

The simplest and most straightforward pattern is the use of ML potentials. There are numerous different kinds of such potentials, including neural networks (NNs) [145], permutationally invariant polynomials (PIPs) [146,147], and delta machine learning (Δ-ML) [148]. These methods produce fitted potentials that are very accurate approximations to first principle ones, but at a much lower cost. They are also easily integrated like the traditional empirical force fields. For IVR calculations, such machine learning potentials replace smoothly the nuclear potentials of the studied systems. No further adjustments are required since we do not need to care about the actual implementations behind the classical propagator. Such utilization of ML potentials has already appeared in IVR applications to open up the possibility for high-precision calculations that involve large numbers of dimensions or trajectories, which directly extends the applicability of the method since they were originally prohibited by the expensive PES evaluations [62,149]. The results are satisfactory and encouraging, which indicates that the ML potentials can be listed as a standard choice for calculations.

Apart from the straightforward replacement of the potential, more involvement and deeper integration of machine learning in the IVR methods have emerged in recent years. This includes determining the Hessian matrix with neural gas algorithm [150] and finding the optimal subspace division in the DC method with evolutionary election [151]. They exploit the strong power of ML in fitting and predicting for more efficient determination of quantities in the IVR framework that used to be computationally costly. Such kind of progress is still in its infancy, and we mention machine learning in this last subsection for its great potential in the next stage of development. This might be one of the most hopeful directions for future improvements where new wisdom will come in to promote its growth.

4. Perspective and conclusion

In this review, we introduced the history and recent developments of the SC-IVR method, including its applications in calculations of vibrational spectroscopy, reaction rate constants, and nonadiabatic dynamics. It is fair to say that even in this century, various improvements have still greatly expanded the scope of its application, and new inspirations are still emerging. As described above, the TA filtering and the MC technique have enhanced the efficiency of utilization of the trajectory samples in different ways. The DC technique reduced the total dimension in a clever manner to avoid the numerical instabilities, while CCFD achieves the same target by shortening the propagation time. These methods and techniques have been combined to study the vibration of many complex systems beyond the reach of other kinds of methods. Other changes including the FB propagation help to calculate the correlation functions and reaction rates with better efficiency. Also, with some modifications it is applicable to nonadiabatic systems with both the electronic states and the nuclei under quantum consideration. Their great performance in describing real-time quantum dynamics foreshadows a promising future as a powerful computational tool.

Despite the significant progress, there also remain challenges to be conquered. The coherent nature of the propagator and the inclusion of phase induce numerical difficulties that are still hard to address completely. The number of dimensions under quantum consideration is limited which always needs careful treatment when considering large and complex systems. Although various improvements like DC, CCFD, and FB have significantly mitigated the negative effects of such behavior, the applicability is still not fully satisfactory. The additional information required in classical evolution also creates a dilemma about accuracy and practicality. The propagation of the monodromy matrix is a hard task requiring more computational effort than traditional molecular dynamics. The fast-growing pre-exponential factor is an essential part of the quantum effects, but it brings about severe numerical problems. The TA averaging and the separable approximation tackle these in a rather elegant way, but the root of numerical difficulties is not solved. Such problems become significant for floppy systems which ask for more detailed adjustments. Further improvements are called for to overcome the difficulty, such as more numerically friendly pre-exponential factors that preserve accuracy. For nonadiabatic systems, the framework is complete but there are issues with realistic applications. The requirements for convergence are more demanding than adiabatic cases, which might be alleviated with better mapping approaches. In general, more compromises are needed on the way of application in large systems, which is an understandable yet still unsatisfying limitation. Efforts still need to be made to push the boundaries further.

We are hopeful about the future in which the challenges will be conquered. Long back ago, the IVR framework was anticipated to address problems in condensed matter, but the high computational cost and large number of DOFs have made highly realistic calculations not doable. Now with the new applications on realistic condensed phase

systems beyond simple models, this long-held expectation seems to be on the verge of becoming a reality. Although the number of cases is still limited currently, the feasibility has been verified. We hope to attract some attention so that more researchers in the field of material science can recognize the potential of this method, expanding the possibilities for further applications with their valuable ideas.

Besides these, a promising direction is the integration of machine learning. The use of ML potentials is the simplest but most viable way for better performance. The ML consideration of other parts of the IVR framework is also showing up. Hopefully in the future, we will be able to handle more difficult ones such as the costly computation of the monodromy matrix, with further improvement in the efficiency and reliability of the method. We believe that the concept of ML will inject fresh inspiration into this field.

In conclusion, the applications of SC-IVR to more challenging problems and improvements toward better efficiency await further exploration. We hope that this review can facilitate interested readers to understand the most fundamental principles underlying this method. With additional advancements in the future, it will hopefully evolve into a highly efficient and effective tool for quantum dynamics, which might surpass the capabilities of many other methods.

CRediT authorship contribution statement

Jia-Xi Zeng: Writing – review & editing, Writing – original draft, Methodology, Data curation, Conceptualization. **Xin-Zheng Li:** Writing – review & editing, Supervision, Project administration, Funding acquisition.

Declaration of competing interest

The authors declare that they have no known competing financial interests or personal relationships that could have appeared to influence the work reported in this paper.

Acknowledgments

We are grateful to the financial support of the National Basic Research Programs of China under Grant Nos. 2021YFA1400500 and 2022YFA1403500, and the National Science Foundation of China under Grant Nos. 12234001, 12474215, and 62321004. The computational resources were provided by the supercomputer center at Peking University, China.

Data availability

Data will be made available on request.

References

[1] M.-P. Gaigeot, M. Sprik, Ab Initio Molecular Dynamics Computation of the Infrared Spectrum of Aqueous Uracil, J. Phys. Chem. B 107 (38) (2003) 10344–10358, http://dx.doi.org/10.1021/jp034788u.

[2] M. Thomas, M. Brehm, R. Fligg, P. Vöhringer, B. Kirchner, Computing vibrational spectra from ab initio molecular dynamics, Phys. Chem. Chem. Phys. 15 (2013) 6608–6622, http://dx.doi.org/10.1039/C3CP44302G.

[3] P.H. Berens, K.R. Wilson, Molecular dynamics and spectra. I. Diatomic rotation and vibration, J. Chem. Phys. 74 (9) (1981) 4872–4882, http://dx.doi.org/10.1063/1.441739.

[4] F.H. Stillinger, T.A. Weber, R.A. LaViolette, Chemical reactions in liquids: Molecular dynamics simulation for sulfur, J. Chem. Phys. 85 (11) (1986) 6460–6469, http://dx.doi.org/10.1063/1.451426.

[5] B. Guillot, A molecular dynamics study of the far infrared spectrum of liquid water, J. Chem. Phys. 95 (3) (1991) 1543–1551, http://dx.doi.org/10.1063/1.461069.

[6] W.B. Bosma, L.E. Fried, S. Mukamel, Simulation of the intermolecular vibrational spectra of liquid water and water clusters, J. Chem. Phys. 98 (6) (1993) 4413–4421, http://dx.doi.org/10.1063/1.465001.

[7] J. Lee, S. Yang, J. Kim, S. Lee, An efficient molecular dynamics simulation method for calculating the diffusion-influenced reaction rates, J. Chem. Phys. 120 (16) (2004) 7564–7575, http://dx.doi.org/10.1063/1.1687680.

[8] R. Alimi, A. García-Vela, R.B. Gerber, A remedy for zero-point energy problems in classical trajectories: A combined semiclassical/classical molecular dynamics algorithm, J. Chem. Phys. 96 (3) (1992) 2034–2038, http://dx.doi.org/10.1063/1.462106.

[9] R.J. McMahon, Chemical reactions involving quantum tunneling, Science 299 (5608) (2003) 833–834, http://dx.doi.org/10.1126/science.1080715.

[10] B. Tremblay, B. Madebène, M. Alikhani, J. Perchard, The vibrational spectrum of the water trimer: Comparison between anharmonic ab initio calculations and neon matrix infrared date between 11,000 and 90cm-1, Chem. Phys. 378 (1) (2010) 27–36, http://dx.doi.org/10.1016/j.chemphys.2010.09.010.

[11] J.O. Richardson, C. Pérez, S. Lobsiger, A.A. Reid, B. Temelso, G.C. Shields, Z. Kisiel, D.J. Wales, B.H. Pate, S.C. Althorpe, Concerted hydrogen-bond breaking by quantum tunneling in the water hexamer prism, Science 351 (6279) (2016) 1310–1313, http://dx.doi.org/10.1126/science.aae0012.

[12] F. Wu, Y. Ren, W. Bian, The hydrogen tunneling splitting in malonaldehyde: A full-dimensional time-independent quantum mechanical method, J. Chem. Phys. 145 (7) (2016) 074309, http://dx.doi.org/10.1063/1.4960789.

[13] R. Wild, M. Nötzold, M. Simpson, T.D. Tran, R. Wester, Tunnelling measured in a very slow ion–molecule reaction, Nature 615 (7952) (2023) 425–429, http://dx.doi.org/10.1038/s41586-023-05727-z.

[14] X.-Z. Li, B. Walker, A. Michaelides, Quantum nature of the hydrogen bond, Proc. Natl. Acad. Sci. USA 108 (16) (2011) 6369–6373, http://dx.doi.org/10.1073/pnas.1016653108.

[15] M. Ceriotti, J. Cuny, M. Parrinello, D.E. Manolopoulos, Nuclear quantum effects and hydrogen bond fluctuations in water, Proc. Natl. Acad. Sci. USA 110 (39) (2013) 15591–15596, http://dx.doi.org/10.1073/pnas.1308560110.

[16] M. Rossi, M. Ceriotti, D.E. Manolopoulos, How to remove the spurious resonances from ring polymer molecular dynamics, J. Chem. Phys. 140 (23) (2014) 234116, http://dx.doi.org/10.1063/1.4883861.

[17] M. Ceriotti, W. Fang, P.G. Kusalik, R.H. McKenzie, A. Michaelides, M.A. Morales, T.E. Markland, Nuclear quantum effects in water and aqueous systems: Experiment, theory, and current challenges, Chem. Rev. 116 (13) (2016) 7529–7550, http://dx.doi.org/10.1021/acs.chemrev.5b00674, PMID: 27049513.

[18] Y. Feng, J. Chen, X.-Z. Li, E. Wang, Ab initio path-integral molecular dynamics and the quantum nature of hydrogen bonds*, Chin. Phys. B 25 (1) (2015) 013104, http://dx.doi.org/10.1088/1674-1056/25/1/013104.

[19] W. Fang, J. Chen, M. Rossi, Y. Feng, X.-Z. Li, A. Michaelides, Inverse temperature dependence of nuclear quantum effects in DNA base pairs, J. Phys. Chem. Lett. 7 (11) (2016) 2125–2131, http://dx.doi.org/10.1021/acs.jpclett.6b00777, PMID: 27195654.

[20] Y. Feng, J. Chen, W. Fang, E.-G. Wang, A. Michaelides, X.-Z. Li, Hydrogenation facilitates proton transfer through two-dimensional honeycomb crystals, J. Phys. Chem. Lett. 8 (24) (2017) 6009–6014, http://dx.doi.org/10.1021/acs.jpclett.7b02820, PMID: 29185752.

[21] W. Fang, J.O. Richardson, J. Chen, X.-Z. Li, A. Michaelides, Simultaneous deep tunneling and classical hopping for hydrogen diffusion on metals, Phys. Rev. Lett. 119 (2017) 126001, http://dx.doi.org/10.1103/PhysRevLett.119.126001.

[22] G.C. Schatz, Quantum effects in gas phase bimolecular chemical reactions, Annu. Rev. Phys. Chem. 39 (1) (1988) 317–340, http://dx.doi.org/10.1146/annurev.pc.39.100188.001533.

[23] D.G. Truhlar, D.W. Schwenke, D.J. Kouri, Quantum dynamics of chemical reactions by converged algebraic variational calculations, J. Phys. Chem. 94 (19) (1990) 7346–7352, http://dx.doi.org/10.1021/j100382a007.

[24] J.C. Light, T. Carrington Jr., Discrete-variable representations and their utilization, in: Adv. Chem. Phys., John Wiley & Sons, Ltd, 2000, pp. 263–310, http://dx.doi.org/10.1002/9780470141731.ch4.

[25] R. Jaquet, Quantum reactive scattering: the time-independent approach. I. principles and early developments, in: W. Jakubetz (Ed.), Methods in Reaction Dynamics, Springer Berlin Heidelberg, Berlin, Heidelberg, 2001, pp. 17–82.

[26] H.-D. Meyer, U. Manthe, L. Cederbaum, The multi-configurational time-dependent Hartree approach, Chem. Phys. Lett. 165 (1) (1990) 73–78, http://dx.doi.org/10.1016/0009-2614(90)87014-I.

[27] U. Manthe, H.-D. Meyer, L.S. Cederbaum, Wave-packet dynamics within the multiconfiguration Hartree framework: General aspects and application to NOCl, J. Chem. Phys. 97 (5) (1992) 3199–3213, http://dx.doi.org/10.1063/1.463007.

[28] M. Beck, H.-D. Meyer, An efficient and robust integration scheme for the equations of motion of the multiconfiguration time-dependent Hartree (MCTDH) method, Z. Phys. D: At. Mol. Clust. 42 (2) (1997) 113–129, http://dx.doi.org/10.1007/s004600050342.

[29] M. Beck, A. Jäckle, G. Worth, H.-D. Meyer, The multiconfiguration time-dependent Hartree (MCTDH) method: a highly efficient algorithm for propagating wavepackets, Phys. Rep. 324 (1) (2000) 1–105, http://dx.doi.org/10.1016/S0370-1573(99)00047-2.

[30] J.M. Bowman, Self-consistent field energies and wavefunctions for coupled oscillators, J. Chem. Phys. 68 (2) (1978) 608–610, http://dx.doi.org/10.1063/1.435782.

[31] J.M. Bowman, K. Christoffel, F. Tobin, Application of SCF-SI theory to vibrational motion in polyatomic molecules, J. Phys. Chem. 83 (8) (1979) 905–912, http://dx.doi.org/10.1021/j100471a005.
[32] K.M. Christoffel, J.M. Bowman, Investigations of self-consistent field, scf ci and virtual state configuration interaction vibrational energies for a model three-mode system, Chem. Phys. Lett. 85 (2) (1982) 220–224, http://dx.doi.org/10.1016/0009-2614(82)80335-7.
[33] S. Carter, S.J. Culik, J.M. Bowman, Vibrational self-consistent field method for many-mode systems: A new approach and application to the vibrations of CO adsorbed on Cu(100), J. Chem. Phys. 107 (24) (1997) 10458–10469, http://dx.doi.org/10.1063/1.474210.
[34] J.M. Bowman, T. Carrington, H.-D. Meyer, Variational quantum approaches for computing vibrational energies of polyatomic molecules, Mol. Phys. 106 (16–18) (2008) 2145–2182, http://dx.doi.org/10.1080/00268970802258609.
[35] R. Grimm, R. Storer, Monte-Carlo solution of Schrödinger's equation, J. Comput. Phys. 7 (1) (1971) 134–156, http://dx.doi.org/10.1016/0021-9991(71)90054-4.
[36] A. Badinski, P.D. Haynes, R.J. Needs, Nodal Pulay terms for accurate diffusion quantum Monte Carlo forces, Phys. Rev. B 77 (2008) 085111, http://dx.doi.org/10.1103/PhysRevB.77.085111.
[37] R.J. Needs, M.D. Towler, N.D. Drummond, P.L. Ríos, Continuum variational and diffusion quantum Monte Carlo calculations, J. Phys.: Condens. Matter. 22 (2) (2009) 023201, http://dx.doi.org/10.1088/0953-8984/22/2/023201.
[38] D.M. Ceperley, Path integrals in the theory of condensed helium, Rev. Modern Phys. 67 (1995) 279–355, http://dx.doi.org/10.1103/RevModPhys.67.279.
[39] R.O. Weht, J. Kohanoff, D.A. Estrin, C. Chakravarty, An ab initio path integral Monte Carlo simulation method for molecules and clusters: Application to Li4 and Li5+, J. Chem. Phys. 108 (21) (1998) 8848–8858, http://dx.doi.org/10.1063/1.476331.
[40] I.R. Craig, D.E. Manolopoulos, Quantum statistics and classical mechanics: Real time correlation functions from ring polymer molecular dynamics, J. Chem. Phys. 121 (8) (2004) 3368–3373, http://dx.doi.org/10.1063/1.1777575.
[41] T.D. Hone, P.J. Rossky, G.A. Voth, A comparative study of imaginary time path integral based methods for quantum dynamics, J. Chem. Phys. 124 (15) (2006) 154103, http://dx.doi.org/10.1063/1.2186636.
[42] A. Witt, S.D. Ivanov, M. Shiga, H. Forbert, D. Marx, On the applicability of centroid and ring polymer path integral molecular dynamics for vibrational spectroscopy, J. Chem. Phys. 130 (19) (2009) 194510, http://dx.doi.org/10.1063/1.3125009.
[43] J.O. Richardson, S.C. Althorpe, Ring-polymer instanton method for calculating tunneling splittings, J. Chem. Phys. 134 (5) (2011) 054109, http://dx.doi.org/10.1063/1.3530589.
[44] J.O. Richardson, S.C. Althorpe, D.J. Wales, Instanton calculations of tunneling splittings for water dimer and trimer, J. Chem. Phys. 135 (12) (2011) 124109, http://dx.doi.org/10.1063/1.3640429.
[45] J.O. Richardson, R. Bauer, M. Thoss, Semiclassical Green's functions and an instanton formulation of electron-transfer rates in the nonadiabatic limit, J. Chem. Phys. 143 (13) (2015) 134115, http://dx.doi.org/10.1063/1.4932361.
[46] J.O. Richardson, Derivation of instanton rate theory from first principles, J. Chem. Phys. 144 (11) (2016) 114106, http://dx.doi.org/10.1063/1.4943866.
[47] J.O. Richardson, Microcanonical and thermal instanton rate theory for chemical reactions at all temperatures, Faraday Discuss. 195 (2016) 49–67, http://dx.doi.org/10.1039/C6FD00119J.
[48] T.J.H. Hele, Quantum Transition-State Theory (Ph.D. thesis), University of Cambridge, 2014.
[49] M.V. Pak, A. Chakraborty, S. Hammes-Schiffer, Density functional theory treatment of electron correlation in the nuclear-electronic orbital approach, J. Phys. Chem. A 111 (20) (2007) 4522–4526, http://dx.doi.org/10.1021/jp0704463.
[50] A. Chakraborty, M.V. Pak, S. Hammes-Schiffer, Development of electron-proton density functionals for multicomponent density functional theory, Phys. Rev. Lett. 101 (2008) 153001, http://dx.doi.org/10.1103/PhysRevLett.101.153001.
[51] A. Chakraborty, M.V. Pak, S. Hammes-Schiffer, Properties of the exact universal functional in multicomponent density functional theory, J. Chem. Phys. 131 (12) (2009) 124115, http://dx.doi.org/10.1063/1.3236844.
[52] I. Errea, M. Calandra, F. Mauri, Anharmonic free energies and phonon dispersions from the stochastic self-consistent harmonic approximation: Application to platinum and palladium hydrides, Phys. Rev. B 89 (2014) 064302, http://dx.doi.org/10.1103/PhysRevB.89.064302.
[53] R. Bianco, I. Errea, L. Paulatto, M. Calandra, F. Mauri, Second-order structural phase transitions, free energy curvature, and temperature-dependent anharmonic phonons in the self-consistent harmonic approximation: Theory and stochastic implementation, Phys. Rev. B 96 (2017) 014111, http://dx.doi.org/10.1103/PhysRevB.96.014111.
[54] L. Monacelli, I. Errea, M. Calandra, F. Mauri, Pressure and stress tensor of complex anharmonic crystals within the stochastic self-consistent harmonic approximation, Phys. Rev. B 98 (2018) 024106, http://dx.doi.org/10.1103/PhysRevB.98.024106.
[55] L. Monacelli, R. Bianco, M. Cherubini, M. Calandra, I. Errea, F. Mauri, The stochastic self-consistent harmonic approximation: calculating vibrational properties of materials with full quantum and anharmonic effects, J. Phys.: Condens. Matter. 33 (36) (2021) 363001, http://dx.doi.org/10.1088/1361-648X/ac066b.
[56] W.H. Miller, Classical S matrix: Numerical application to inelastic collisions, J. Chem. Phys. 53 (9) (1970) 3578–3587, http://dx.doi.org/10.1063/1.1674535.
[57] M.F. Herman, E. Kluk, A semiclasical justification for the use of non-spreading wavepackets in dynamics calculations, Chem. Phys. 91 (1) (1984) 27–34, http://dx.doi.org/10.1016/0301-0104(84)80039-7.
[58] J.H. van Vleck, The correspondence principle in the statistical interpretation of quantum mechanics, Proc. Natl. Acad. Sci. USA 14 (2) (1928) 178–188, http://dx.doi.org/10.1073/pnas.14.2.178.
[59] W.H. Miller, The semiclassical initial value representation: A potentially practical way for adding quantum effects to calssical molecular dynamics simulations, J. Phys. Chem. A 105 (13) (2001) 2942–2955, http://dx.doi.org/10.1021/jp003712k.
[60] A.L. Kaledin, W.H. Miller, Time averaging the semiclassical initial value representation for the calculation of vibrational energy levels. II. Application to H2CO,NH3, CH4,CH2D2, J. Chem. Phys. 119 (6) (2003) 3078–3084, http://dx.doi.org/10.1063/1.1589477.
[61] M. Ceotto, G. Di Liberto, R. Conte, Semiclassical "divide-and-conquer" method for spectroscopic calculations of high dimensional molecular systems, Phys. Rev. Lett. 119 (2017) 010401, http://dx.doi.org/10.1103/PhysRevLett.119.010401.
[62] J.-X. Zeng, S. Yang, Y.-C. Zhu, W. Fang, L. Jiang, E.-G. Wang, D.H. Zhang, X.-Z. Li, Semiclassical vibrational spectroscopy of real molecular systems by means of cross-correlation filter diagonalization, J. Phys. Chem. A 127 (13) (2023) 2902–2911, http://dx.doi.org/10.1021/acs.jpca.3c00576.
[63] A.L. Kaledin, W.H. Miller, Time averaging the semiclassical initial value representation for the calculation of vibrational energy levels, J. Chem. Phys. 118 (16) (2003) 7174–7182, http://dx.doi.org/10.1063/1.1562158.
[64] M. Buchholz, F. Grossmann, M. Ceotto, Simplified approach to the mixed time-averaging semiclassical initial value representation for the calculation of dense vibrational spectra, J. Chem. Phys. 148 (11) (2018) 114107, http://dx.doi.org/10.1063/1.5020144.
[65] M. Ceotto, S. Atahan, G.F. Tantardini, A. Aspuru-Guzik, Multiple coherent states for first-principles semiclassical initial value representation molecular dynamics, J. Chem. Phys. 130 (23) (2009) 234113, http://dx.doi.org/10.1063/1.3155062.
[66] M. Ceotto, G.F. Tantardini, A. Aspuru-Guzik, Fighting the curse of dimensionality in first-principles semiclassical calculations: Non-local reference states for large number of dimensions, J. Chem. Phys. 135 (21) (2011) 214108, http://dx.doi.org/10.1063/1.3664731.
[67] F. Gabas, R. Conte, M. Ceotto, Semiclassical vibrational spectroscopy of biological molecules using force fields, J. Chem. Theory Comput. 16 (6) (2020) 3476–3485, http://dx.doi.org/10.1021/acs.jctc.0c00127.
[68] G. Di Liberto, R. Conte, M. Ceotto, "Divide and conquer" semiclassical molecular dynamics: A practical method for spectroscopic calculations of high dimensional molecular systems, J. Chem. Phys. 148 (1) (2018) 014307, http://dx.doi.org/10.1063/1.5010388.
[69] G. Di Liberto, R. Conte, M. Ceotto, "Divide-and-conquer" semiclassical molecular dynamics: An application to water clusters, J. Chem. Phys. 148 (10) (2018) 104302, http://dx.doi.org/10.1063/1.5023155.
[70] R. Conte, L. Parma, C. Aieta, A. Rognoni, M. Ceotto, Improved semiclassical dynamics through adiabatic switching trajectory sampling, J. Chem. Phys. 151 (21) (2019) 214107, http://dx.doi.org/10.1063/1.5133144.
[71] G. Botti, M. Ceotto, R. Conte, On-the-fly adiabatically switched semiclassical initial value representation molecular dynamics for vibrational spectroscopy of biomolecules, J. Chem. Phys. 155 (23) (2021) 234102, http://dx.doi.org/10.1063/5.0075220.
[72] D.E. Skinner, W.H. Miller, Application of the semiclassical initial value representation and its linearized approximation to inelastic scattering, Chem. Phys. Lett. 300 (1) (1999) 20–26, http://dx.doi.org/10.1016/S0009-2614(98)01290-1.
[73] Y. Zhao, W.H. Miller, Semiclassical initial value representation for the Boltzmann operator in thermal rate constants, J. Chem. Phys. 117 (21) (2002) 9605–9610, http://dx.doi.org/10.1063/1.1517044.
[74] T. Yamamoto, H. Wang, W.H. Miller, Combining semiclassical time evolution and quantum Boltzmann operator to evaluate reactive flux correlation function for thermal rate constants of complex systems, J. Chem. Phys. 116 (17) (2002) 7335–7349, http://dx.doi.org/10.1063/1.1464539.
[75] W.H. Miller, Quantum mechanical transition state theory and a new semiclassical model for reaction rate constants, J. Chem. Phys. 61 (5) (1974) 1823–1834, http://dx.doi.org/10.1063/1.1682181.
[76] J.-X. Zeng, X.-Z. Li, Semiclassical reaction rate constant of non-adiabatic system by means of initial value representation, AIP Adv. 14 (3) (2024) 035023, http://dx.doi.org/10.1063/5.0200052.
[77] X. Sun, H. Wang, W.H. Miller, Semiclassical theory of electronically nonadiabatic dynamics: Results of a linearized approximation to the initial value representation, J. Chem. Phys. 109 (17) (1998) 7064–7074, http://dx.doi.org/10.1063/1.477389.
[78] W.H. Miller, Classical path approximation for the Boltzmann density matrix, J. Chem. Phys. 55 (7) (1971) 3146–3149, http://dx.doi.org/10.1063/1.1676560.
[79] H.-D. Meyer, W.H. Miller, A classical analog for electronic degrees of freedom in nonadiabatic collision processes, J. Chem. Phys. 70 (7) (1979) 3214–3223, http://dx.doi.org/10.1063/1.437910.

[80] G. Stock, M. Thoss, Semiclassical description of nonadiabatic quantum dynamics, Phys. Rev. Lett. 78 (1997) 578–581, http://dx.doi.org/10.1103/PhysRevLett.78.578.
[81] X. Sun, W.H. Miller, Semiclassical initial value representation for electronically nonadiabatic molecular dynamics, J. Chem. Phys. 106 (15) (1997) 6346–6353, http://dx.doi.org/10.1063/1.473624.
[82] W.H. Miller, Electronically nonadiabatic dynamics via semiclassical initial value methods, J. Phys. Chem. A 113 (8) (2009) 1405–1415, http://dx.doi.org/10.1021/jp809907p.
[83] G. Tao, Electronically nonadiabatic dynamics in complex molecular systems: An efficient and accurate semiclassical solution, J. Phys. Chem. A 117 (28) (2013) 5821–5825, http://dx.doi.org/10.1021/jp404856p.
[84] H.A. Kramers, Wellenmechanik und halbzahlige quantisierung, Z. Phys. 39 (10) (1926) 828–840, http://dx.doi.org/10.1007/BF01451751.
[85] G. Wentzel, Eine verallgemeinerung der quantenbedingungen für die zwecke der wellenmechanik, Z. Phys. 38 (6) (1926) 518–529, http://dx.doi.org/10.1007/BF01397171.
[86] M. de Gosson, B. Hiley, Short-time quantum propagator and Bohmian trajectories, Phys. Lett. A 377 (42) (2013) 3005–3008, http://dx.doi.org/10.1016/j.physleta.2013.08.031.
[87] R.G. Littlejohn, The Van Vleck formula, Maslov theory, and phase space geometry, J. Stat. Phys. 68 (1) (1992) 7–50, http://dx.doi.org/10.1007/BF01048836.
[88] M.C. Gutzwiller, Phase-integral approximation in momentum space and the bound states of an atom, J. Math. Phys. 8 (10) (1967) 1979–2000, http://dx.doi.org/10.1063/1.1705112.
[89] K.G. Kay, Semiclassical tunneling in the initial value representation, J. Chem. Phys. 107 (7) (1997) 2313–2328, http://dx.doi.org/10.1063/1.475143.
[90] R.A. Marcus, Theory of semiclassical transition probabilities (S matrix) for inelastic and reactive collisions. Uniformization with elastic collision trajectories, J. Chem. Phys. 56 (7) (1972) 3548–3550, http://dx.doi.org/10.1063/1.1677730.
[91] H. Kreek, R.A. Marcus, Semiclassical collision theory. Multidimensional integral method, J. Chem. Phys. 61 (8) (1974) 3308–3312, http://dx.doi.org/10.1063/1.1682492.
[92] E.J. Heller, Cellular dynamics: A new semiclassical approach to time-dependent quantum mechanics, J. Chem. Phys. 94 (4) (1991) 2723–2729, http://dx.doi.org/10.1063/1.459848.
[93] W.H. Miller, Comment on: Semiclassical time evolution without root searches, J. Chem. Phys. 95 (12) (1991) 9428–9430, http://dx.doi.org/10.1063/1.461177.
[94] W.H. Miller, Classical-Limit Quantum Mechanics and the Theory of Molecular Collisions, in: Adv. Chem. Phys., John Wiley & Sons, Ltd, 1974, pp. 69–177, http://dx.doi.org/10.1002/9780470143773.ch2.
[95] J. Ankerhold, M. Saltzer, E. Pollak, A study of the semiclassical initial value representation at short times, J. Chem. Phys. 116 (14) (2002) 5925–5932, http://dx.doi.org/10.1063/1.1458924.
[96] S.A. Deshpande, G.S. Ezra, On the derivation of the Herman–Kluk propagator, J. Phys. A: Math. Gen. 39 (18) (2006) 5067, http://dx.doi.org/10.1088/0305-4470/39/18/020.
[97] W.H. Miller, An alternate derivation of the Herman—Kluk (coherent state) semiclassical initial value representation of the time evolution operator, Mol. Phys. 100 (4) (2002) 397–400, http://dx.doi.org/10.1080/00268970110069029.
[98] K.G. Kay, Integral expressions for the semiclassical time-dependent propagator, J. Chem. Phys. 100 (6) (1994) 4377–4392, http://dx.doi.org/10.1063/1.466320.
[99] K.G. Kay, Semiclassical initial value treatments of atoms and molecules, Annu. Rev. Phys. Chem. 56 (Volume 56, 2005) (2005) 255–280, http://dx.doi.org/10.1146/annurev.physchem.56.092503.141257.
[100] K.G. Kay, The Herman–Kluk approximation: Derivation and semiclassical corrections, Chem. Phys. 322 (1) (2006) 3–12, http://dx.doi.org/10.1016/j.chemphys.2005.06.019.
[101] G. Di Liberto, M. Ceotto, The importance of the pre-exponential factor in semiclassical molecular dynamics, J. Chem. Phys. 145 (14) (2016) 144107, http://dx.doi.org/10.1063/1.4964308.
[102] Q. Shi, E. Geva, A relationship between semiclassical and centroid correlation functions, J. Chem. Phys. 118 (18) (2003) 8173–8184, http://dx.doi.org/10.1063/1.1564814.
[103] W.H. Miller, Perspective: Quantum or classical coherence? J. Chem. Phys. 136 (21) (2012) 210901, http://dx.doi.org/10.1063/1.4727849.
[104] D. Moscato, G. Mandelli, M. Bondanza, F. Lipparini, R. Conte, B. Mennucci, M. Ceotto, Unraveling water solvation effects with quantum mechanics/molecular mechanics semiclassical vibrational spectroscopy: The case of thymidine, J. Am. Chem. Soc. 146 (12) (2024) 8179–8188, http://dx.doi.org/10.1021/jacs.3c12700, PMID: 38470354.
[105] M. Cazzaniga, M. Micciarelli, F. Moriggi, A. Mahmoud, F. Gabas, M. Ceotto, Anharmonic calculations of vibrational spectra for molecular adsorbates: A divide-and-conquer semiclassical molecular dynamics approach, J. Chem. Phys. 152 (10) (2020) 104104, http://dx.doi.org/10.1063/1.5142682.
[106] R. Gelabert, X. Giménez, M. Thoss, H. Wang, W.H. Miller, A log-derivative formulation of the prefactor for the semiclassical Herman-Kluk propagator, J. Phys. Chem. A 104 (45) (2000) 10321–10327, http://dx.doi.org/10.1021/jp0012451.
[107] S. Garashchuk, J.C. Light, Simplified calculation of the stability matrix for semiclassical propagation, J. Chem. Phys. 113 (21) (2000) 9390–9392, http://dx.doi.org/10.1063/1.1321032.
[108] R. Conte, F. Gabas, G. Botti, Y. Zhuang, M. Ceotto, Semiclassical vibrational spectroscopy with Hessian databases, J. Chem. Phys. 150 (24) (2019) 244118, http://dx.doi.org/10.1063/1.5109086.
[109] T. Markovich, S.M. Blau, J.N. Sanders, A. Aspuru-Guzik, Benchmarking compressed sensing, super-resolution, and filter diagonalization, Int. J. Quantum Chem. 116 (14) (2016) 1097–1106, http://dx.doi.org/10.1002/qua.25144.
[110] M.R. Wall, D. Neuhauser, Extraction, through filter-diagonalization, of general quantum eigenvalues or classical normal mode frequencies from a small number of residues or a short-time segment if a signal. I. Theory and application to a quantum-dynamics model, J. Chem. Phys. 102 (20) (1995) 8011–8022, http://dx.doi.org/10.1063/1.468999.
[111] V.A. Mandelshtam, H.S. Taylor, Harmonic inversion of time signals and its applications, J. Chem. Phys. 107 (17) (1997) 6756–6769, http://dx.doi.org/10.1063/1.475324.
[112] V. Mandelshtam, FDM: the filter diagonalization method for data processing in NMR experiments, Prog. Nucl. Magn. Reson. Spectrosc. 38 (2) (2001) 159–196, http://dx.doi.org/10.1016/S0079-6565(00)00032-7.
[113] S. Carter, H.M. Shnider, J.M. Bowman, Variational calculations of rovibrational energies of CH4 and isotopomers in full dimensionality using an ab initio potential, J. Chem. Phys. 110 (17) (1999) 8417–8423, http://dx.doi.org/10.1063/1.478750.
[114] E. Narevicius, D. Neuhauser, H. Jürgen Korsch, N. Moiseyev, Resonances from short time complex-scaled cross-correlation probability amplitudes by the filter-diagonalization method, Chem. Phys. Lett. 276 (3) (1997) 250–254, http://dx.doi.org/10.1016/S0009-2614(97)00867-1.
[115] S.M. Anderson, J. Ka, P.M. Felker, D. Neuhuaser, Semi-classical versus exact eigenvalues of He-benzene using cross-correlation filter-diagonalization, Chem. Phys. Lett. 328 (4) (2000) 516–521, http://dx.doi.org/10.1016/S0009-2614(00)00934-9.
[116] K. Giese, O. Kühn, Semiclassical tunneling splittings from short time dynamics: Herman-Kluk-propagation and harmonic inversion, J. Chem. Phys. 120 (9) (2004) 4107–4118, http://dx.doi.org/10.1063/1.1643734.
[117] T.J. Lee, J.M.L. Martin, P.R. Taylor, An accurate ab initio quartic force field and vibrational frequencies for CH4 and isotopomers, J. Chem. Phys. 102 (1) (1995) 254–261, http://dx.doi.org/10.1063/1.469398.
[118] E. Pollak, J. Shao, Systematic improvement of initial value representations of the semiclassical propagator, J. Phys. Chem. A 107 (37) (2003) 7112–7117, http://dx.doi.org/10.1021/jp030098e.
[119] S. Zhang, E. Pollak, Monte Carlo method for evaluating the quantum real time propagator, Phys. Rev. Lett. 91 (2003) 190201, http://dx.doi.org/10.1103/PhysRevLett.91.190201.
[120] S. Zhang, E. Pollak, Optimization of the semiclassical initial value representation of the exact quantum-mechanical real time propagator, J. Chem. Phys. 119 (21) (2003) 11058–11063, http://dx.doi.org/10.1063/1.1622931.
[121] S. Zhang, E. Pollak, A prefactor free semiclassical initial value series representation of the propagator, J. Chem. Phys. 121 (8) (2004) 3384–3392, http://dx.doi.org/10.1063/1.1772361.
[122] L. de Broglie, La nouvelle dynamique des quanta, in "cinquieme conseil de physique solvay"(bruxelles 1927), ed, J. Bordet,(Gauthier- Villars, Paris, 1928) (1928) 374–406.
[123] D. Bohm, A suggested interpretation of the quantum theory in terms of "hidden" variables. I, Phys. Rev. 85 (1952) 166–179, http://dx.doi.org/10.1103/PhysRev.85.166.
[124] S. Garashchuk, V. Rassolov, O. Prezhdo, Semiclassical bohmian dynamics, in: Reviews in Computational Chemistry, John Wiley & Sons, Ltd, 2010, pp. 287–368, http://dx.doi.org/10.1002/9780470890905.ch6.
[125] L.E. Cook, J.E. Runeson, J.O. Richardson, T.J.H. Hele, Which algorithm best propagates the meyer–Miller–Stock–Thoss mapping Hamiltonian for nonadiabatic dynamics? J. Chem. Theory Comput. 19 (18) (2023) 6109–6125, http://dx.doi.org/10.1021/acs.jctc.3c00709.
[126] M.F. Herman, A semiclassical surface hopping propagator for nonadiabatic problems, J. Chem. Phys. 103 (18) (1995) 8081–8097, http://dx.doi.org/10.1063/1.470173.
[127] Y. Wu, M.F. Herman, Nonadiabatic surface hopping Herman-Kluk semiclassical initial value representation method revisited: Applications to Tully's three model systems, J. Chem. Phys. 123 (14) (2005) 144106, http://dx.doi.org/10.1063/1.2049251.
[128] Y. Wu, M.F. Herman, A justification for a nonadiabatic surface hopping Herman-Kluk semiclassical initial value representation of the time evolution operator, J. Chem. Phys. 125 (15) (2006) 154116, http://dx.doi.org/10.1063/1.2358352.
[129] H. Wang, X. Sun, W.H. Miller, Semiclassical approximations for the calculation of thermal rate constants for chemical reactions in complex molecular systems, J. Chem. Phys. 108 (23) (1998) 9726–9736, http://dx.doi.org/10.1063/1.476447.

[130] N. Makri, K. Thompson, Semiclassical influence functionals for quantum systems in anharmonic environments, Chem. Phys. Lett. 291 (1) (1998) 101–109, http://dx.doi.org/10.1016/S0009-2614(98)00590-9.
[131] J. Shao, N. Makri, Forward-backward semiclassical dynamics without prefactors, J. Phys. Chem. A 103 (39) (1999) 7753–7756, http://dx.doi.org/10.1021/jp991433v.
[132] J. Shao, N. Makri, Forward–backward semiclassical dynamics in the interaction representation, J. Chem. Phys. 113 (9) (2000) 3681–3685, http://dx.doi.org/10.1063/1.1287823.
[133] H. Wang, M. Thoss, W.H. Miller, Forward–backward initial value representation for the calculation of thermal rate constants for reactions in complex molecular systems, J. Chem. Phys. 112 (1) (2000) 47–55, http://dx.doi.org/10.1063/1.480560.
[134] M. Thoss, H. Wang, W.H. Miller, Generalized forward–backward initial value representation for the calculation of correlation functions in complex systems, J. Chem. Phys. 114 (21) (2001) 9220–9235, http://dx.doi.org/10.1063/1.1359242.
[135] E. Bukhman, N. Makri, Forward-backward semiclassical dynamics with information-guided noise reduction for a molecule in solution, J. Phys. Chem. A 111 (44) (2007) 11320–11327, http://dx.doi.org/10.1021/jp0721907, PMID: 17658736.
[136] J. Shao, N. Makri, Forward-backward semiclassical dynamics with linear scaling, J. Phys. Chem. A 103 (47) (1999) 9479–9486, http://dx.doi.org/10.1021/jp991837n.
[137] O. Kühn, N. Makri, Forward-backward semiclassical calculation of spectral line shapes: I2 in a rare gas cluster, J. Phys. Chem. A 103 (47) (1999) 9487–9493, http://dx.doi.org/10.1021/jp991836v.
[138] M. Thoss, H. Wang, Semiclassical description of molecular dynamics based on initial-value representation methods, Annu. Rev. Phys. Chem. 55 (Volume 55, 2004) (2004) 299–332, http://dx.doi.org/10.1146/annurev.physchem.55.091602.094429.
[139] N. Ananth, C. Venkataraman, W.H. Miller, Semiclassical description of electronically nonadiabatic dynamics via the initial value representation, J. Chem. Phys. 127 (8) (2007) 084114, http://dx.doi.org/10.1063/1.2759932.
[140] E. Jezek, N. Makri, Finite temperature correlation functions via forward-backward semiclassical dynamics, J. Phys. Chem. A 105 (12) (2001) 2851–2857, http://dx.doi.org/10.1021/jp003838h.
[141] J. Liu, N. Makri, Symmetries and detailed balance in forward–backward semiclassical dynamics, Chem. Phys. 322 (1) (2006) 23–29, http://dx.doi.org/10.1016/j.chemphys.2005.08.010, Real-time dynamics in complex quantum systems.
[142] J. Liu, A. Nakayama, N. Makri, Long-time behaviour of quantized distributions in forward–backward semiclassical dynamics, Mol. Phys. 104 (8) (2006) 1267–1274, http://dx.doi.org/10.1080/00268970500525754.
[143] N. Makri, Forward–backward semiclassical and quantum trajectory methods for time correlation functions, Phys. Chem. Chem. Phys. 13 (2011) 14442–14452, http://dx.doi.org/10.1039/C0CP02374D.
[144] J. Liu, Recent advances in the linearized semiclassical initial value representation/classical wigner model for the thermal correlation function, Int. J. Quantum Chem. 115 (11) (2015) 657–670, http://dx.doi.org/10.1002/qua.24872.
[145] K. Shao, J. Chen, Z. Zhao, D.H. Zhang, Communication: Fitting potential energy surfaces with fundamental invariant neural network, J. Chem. Phys. 145 (7) (2016) 071101, http://dx.doi.org/10.1063/1.4961454.
[146] B.J. Braams, J.M. Bowman, Permutationally invariant potential energy surfaces in high dimensionality, Int. Rev. Phys. Chem. 28 (4) (2009) 577–606, http://dx.doi.org/10.1080/01442350903234923.
[147] C. Qu, J.M. Bowman, A fragmented, permutationally invariant polynomial approach for potential energy surfaces of large molecules: Application to N-methyl acetamide, J. Chem. Phys. 150 (14) (2019) 141101, http://dx.doi.org/10.1063/1.5092794.
[148] R. Ramakrishnan, P.O. Dral, M. Rupp, O.A. von Lilienfeld, Big data meets quantum chemistry approximations: The δ-machine learning approach, J. Chem. Theory Comput. 11 (5) (2015) 2087–2096, http://dx.doi.org/10.1021/acs.jctc.5b00099, PMID: 26574412.
[149] R. Conte, A. Nandi, C. Qu, Q. Yu, P.L. Houston, J.M. Bowman, Semiclassical and VSCF/VCI calculations of the vibrational energies of trans- and gauche-Ethanol using a CCSD(T) potential energy surface, J. Phys. Chem. A 126 (42) (2022) 7709–7718, http://dx.doi.org/10.1021/acs.jpca.2c06322, PMID: 36240438.
[150] M. Gandolfi, M. Ceotto, Unsupervised machine learning neural gas algorithm for accurate evaluations of the hessian matrix in molecular dynamics, J. Chem. Theory Comput. 17 (11) (2021) 6733–6746, http://dx.doi.org/10.1021/acs.jctc.1c00707, PMID: 34705463.
[151] M. Gandolfi, A. Rognoni, C. Aieta, R. Conte, M. Ceotto, Machine learning for vibrational spectroscopy via divide-and-conquer semiclassical initial value representation molecular dynamics with application to N-methylacetamide, J. Chem. Phys. 153 (20) (2020) 204104, http://dx.doi.org/10.1063/5.0031892.